

Mean Field Limit of the Learning Dynamics of Multilayer Neural Networks

Phan-Minh Nguyen*

February 11, 2019

Abstract

Can multilayer neural networks – typically constructed as highly complex structures with many nonlinearly activated neurons across layers – behave in a non-trivial way that yet simplifies away a major part of their complexities? In this work, we uncover a phenomenon in which the behavior of these complex networks – under suitable scalings and stochastic gradient descent dynamics – becomes independent of the number of neurons as this number grows sufficiently large. We develop a formalism in which this many-neurons limiting behavior is captured by a set of equations, thereby exposing a previously unknown operating regime of these networks. While the current pursuit is mathematically non-rigorous, it is complemented with several experiments that validate the existence of this behavior.

1 Introduction

The breakthrough empirical success of deep learning [LBH15] has spurred strong interests in theoretical understanding of multilayer neural networks. Recent progresses have been made from various perspectives within and beyond traditional learning-theoretic frameworks and tools – a very incomplete list of references includes [ABGM14, CHM⁺15, MP16, SS16, Mal16, SGGSD17, ZSJ⁺17, SZT17, SJJ18, NH18, GSd⁺18, HNP⁺18, WLLM18]. Analyzing these networks is challenging due to their inherent complexities, first as highly nonlinear structures, usually involving a large number of neurons at each layer, and second as highly non-convex optimization problems, typically solved by gradient-based learning rules without strong guarantees. One question then arises: given such complex nature, is it possible to obtain a succinct description of their behavior?

In this work, we show that under suitable scalings and stochastic gradient descent (SGD) learning dynamics, the behavior of a multilayer neural network tends to a non-trivial limit as its number of neurons approaches infinity. We refer to this limit as the *mean field (MF) limit*. In this limit, the complexity of the network becomes independent of the number of neurons, and the network admits a simplified description that depends only on other intrinsic characteristics, such as the number of layers and the data distribution. Interestingly this implies that two networks, which differ by the number of neurons and hence the degree of over-parameterization, can perform almost equally, so long as both have sufficiently many neurons. A similar phenomenon has been recently discovered and studied in two-layers neural networks [MMN18, CB18b, RVE18, SS18a].

*Department of Electrical Engineering, Stanford University.

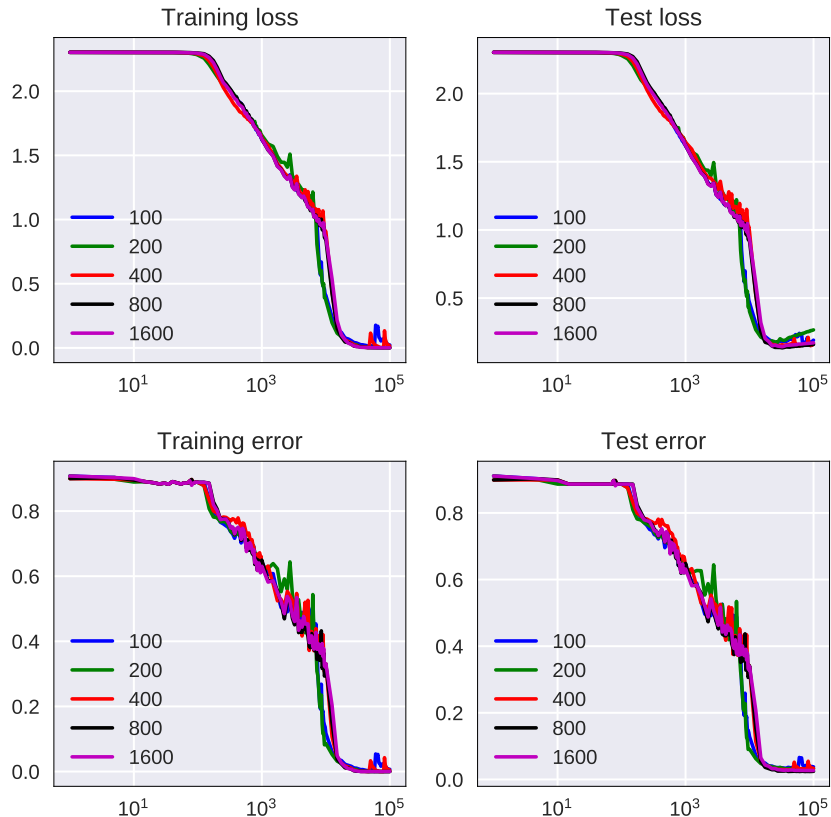


Figure 1: The performance of five 4-layers fully-connected networks on MNIST classification, plotted against training iterations. The number of neurons at each hidden layer is 100, 200, 400, 800 or 1600, for each network. Details are available in Section 4.

To give a glimpse into the MF limit, in Fig. 1, we plot the evolution of the performance of several 4-layers networks, each with a distinct number of neurons per layer, on the MNIST classification task, under the chosen scalings. Observe how well the curves with large numbers of neurons coincide, while the networks still achieve non-trivial performance.

In the following, we shall give a motivating example via the two-layers network case, before presenting the contributions of our work, discussing related works and outlining the rest of the paper. Before we proceed, we introduce some mathematical conventions.

1.1 Notations, definitions and conventions

We use boldface letters to denote vectors if lowercase (e.g. \mathbf{x} , $\boldsymbol{\theta}$) and matrices if uppercase (e.g. \mathbf{W}). For $n \in \mathbb{N}_{>0}$, we use $[n]$ to denote the set $\{1, 2, \dots, n\}$. For a scalar mapping $f : \mathbb{R} \mapsto \mathbb{R}$ and a vector $\mathbf{u} \in \mathbb{R}^n$, we use $f(\mathbf{u})$ to denote $(f(u_1), \dots, f(u_n))^T$ entry-wise. For two vectors $\mathbf{u}, \mathbf{v} \in \mathbb{R}^n$, $\langle \mathbf{u}, \mathbf{v} \rangle$ denotes the usual Euclidean inner product. For a set $E \subseteq \mathbb{R}$ and $x \in \mathbb{R}$, we use $E + x$ to denote $\{u + x : u \in E\}$.

We reserve the notation $\mathcal{P}(\Omega)$ for the set of probability measures on the set Ω . Strictly speaking,

one should associate Ω with a sigma-algebra to define $\mathcal{P}(\Omega)$. We ignore this important technical fact in this paper. We will also make use of the concept of stochastic kernels: ν is a stochastic kernel¹ with a source set Ω (associated with a sigma-algebra \mathcal{F}) and a target set S (associated with a sigma-algebra \mathcal{S}) if $\nu(\cdot|\cdot)$ is a mapping $\mathcal{S} \times \Omega \mapsto [0, 1]$ such that $\nu(\cdot|\omega) \in \mathcal{P}(S)$ for each $\omega \in \Omega$ and $\nu(E|\cdot)$ is \mathcal{F} -measurable for each $E \in \mathcal{S}$. We reserve the notation $\mathcal{K}(\Omega, S)$ for the set of all such kernels. For a stochastic kernel $\nu \in \mathcal{K}(\Omega, S)$, we define

$$\text{CE}\{\nu\}(\cdot) = \int_S x \nu(dx|\cdot),$$

i.e. the conditional expectation operator. We assume that $\text{CE}\{\nu\}$ exists almost everywhere for all stochastic kernels ν to be considered in the paper.

We use $\text{Emp}(\{x_i\}_{i \in [n]})$ to denote the empirical distribution $(1/n) \cdot \sum_{i=1}^n \delta_{x_i}$. For a random variable X , the distributional law of X is denoted by $\text{Law}(X)$. For a measure μ , we use $\text{supp}(\mu)$ to denote its support. A statement of the form $A(x) = B(x)$ for μ -a.e. x for a probability measure μ means that

$$\int A(x) \phi(x) \mu(dx) = \int B(x) \phi(x) \mu(dx)$$

for all smooth and bounded ϕ .

For a functional $f: \mathcal{F} \mapsto \mathbb{R}$ on a suitable vector space \mathcal{F} , we use $\mathcal{D}f$ to denote its differential: for each $g \in \mathcal{F}$, $\mathcal{D}f\{g\}$ is a linear functional from \mathcal{F} to \mathbb{R} such that

$$\lim_{\epsilon \rightarrow 0} \frac{1}{\epsilon} (f(g + \epsilon\varphi) - f(g)) = \mathcal{D}f\{g\}(\varphi)$$

for $\varphi \in \mathcal{F}$. We shall ignore the fact that \mathcal{F} is not arbitrary for this concept to apply.

A subscript in the differential operator (∂ , ∇ or \mathcal{D}) indicates the partial differentiation w.r.t. the respective argument. For example, for $f(u, \mathbf{v}, g): \mathbb{R} \times \mathbb{R}^m \times \mathcal{F} \mapsto \mathbb{R}$ where \mathcal{F} is a set of functions, we use $\partial_1 f$, $\nabla_2 f$ and $\mathcal{D}_3 f$ (or $\partial_u f$, $\nabla_v f$ and $\mathcal{D}_g f$ respectively) to denote its partial derivative w.r.t. u , \mathbf{v} and g respectively.

We use $\|\mathbf{u}\|_2$ to denote the Euclidean norm of a vector \mathbf{u} , $\|\mathbf{W}\|_F$ the Frobenius norm of a matrix \mathbf{W} and $\|f\|_\infty$ the max norm of a function f .

1.2 A motivating example: two-layers neural networks

We give a brief and informal overview of relevant results from [MMN18]. Consider the following two-layers neural network:

$$\hat{y}_n(\mathbf{x}; \mathcal{W}) = \frac{1}{n} \sum_{i=1}^n \sigma(\mathbf{x}; \boldsymbol{\theta}_i), \quad (1)$$

where $\mathbf{x} \in \mathbb{R}^d$ is the input, $\mathcal{W} = \{\boldsymbol{\theta}_i\}_{i \in [n]}$ is the collection of weights $\boldsymbol{\theta}_i \in \mathbb{R}^D$, and $\sigma: \mathbb{R}^d \times \mathbb{R}^D \mapsto \mathbb{R}$ is the (nonlinear) activation. Here each term $\sigma(\mathbf{x}; \boldsymbol{\theta}_i)$ is a neuron. With $\boldsymbol{\theta}_i = (\beta_i, \mathbf{w}_i, b_i) \in \mathbb{R} \times \mathbb{R}^d \times \mathbb{R}$ and $\sigma(\mathbf{x}; \boldsymbol{\theta}_i) = \beta_i \varphi(\langle \mathbf{w}_i, \mathbf{x} \rangle + b_i)$ for a scalar nonlinearity φ , this network reduces to the usual two-layers fully-connected neural network. An illustration is given in Fig. 2.

Suppose that at each time $k \in \mathbb{N}$, the data $(\mathbf{x}^k, y^k) \in \mathbb{R}^d \times \mathbb{R}$ is drawn independently from a probabilistic source \mathcal{P} . We train the network with the loss $\mathcal{L}(y, \hat{y}_n(\mathbf{x}; \mathcal{W}))$ for a loss function

¹Not to be confused with a kernel function that is randomly generated.

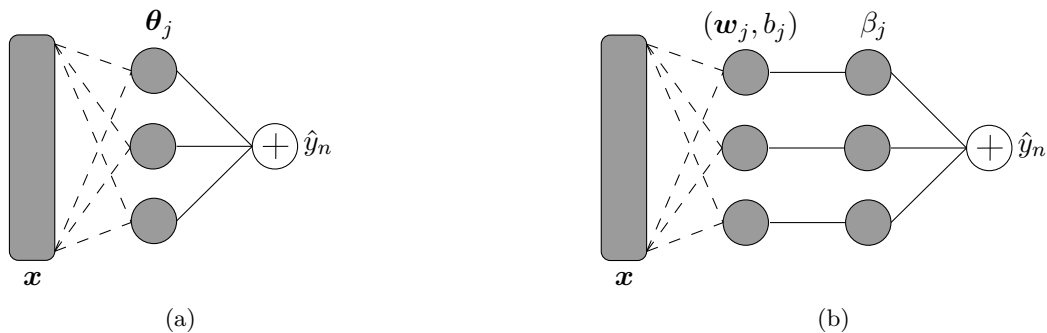


Figure 2: (a): A graphical representation of a two-layer network, as in Eq. (1). (b): An equivalent representation for $\sigma(\mathbf{x}; \boldsymbol{\theta}_i) = \beta_i \varphi(\langle \mathbf{w}_i, \mathbf{x} \rangle + b_i)$.

$\mathcal{L} : \mathbb{R} \times \mathbb{R} \mapsto \mathbb{R}$. In particular, starting from an initialization $\mathcal{W}^0 = \{\boldsymbol{\theta}_i^0\}_{i \in [n]}$, for a learning rate $\alpha > 0$, we perform (discrete-time) SGD:

$$\boldsymbol{\theta}_i^{k+1} = \boldsymbol{\theta}_i^k - \alpha n \nabla_{\boldsymbol{\theta}_i} \mathcal{L}(y^k, \hat{y}_n(\mathbf{x}^k; \mathcal{W}^k)) = \boldsymbol{\theta}_i^k - \alpha \partial_2 \mathcal{L}(y^k, \hat{y}_n(\mathbf{x}^k; \mathcal{W}^k)) \nabla_{\boldsymbol{\theta}} \sigma(\mathbf{x}^k; \boldsymbol{\theta}_i^k). \quad (2)$$

We take a note on the scalings by n in Eq. (1) and (2). The MF limit behavior can then be observed in the following two senses: statics and dynamics.

Statics.

Observe that the sum in (1) exhibits symmetry in the role of the neurons. In the limit $n \rightarrow \infty$, one can replace this sum with an integral:

$$\hat{y}(\mathbf{x}; \rho) = \int \sigma(\mathbf{x}; \boldsymbol{\theta}) \rho(d\boldsymbol{\theta}), \quad (3)$$

for $\rho \in \mathcal{P}(\mathbb{R}^D)$. In particular, on one hand, for a given \mathcal{W} , the identification $\rho = \text{Emp}(\{\boldsymbol{\theta}_i\}_{i \in [n]})$ results in $\hat{y}(\mathbf{x}; \rho) = \hat{y}_n(\mathbf{x}; \mathcal{W})$. On the other hand, for a given ρ , taking $\boldsymbol{\theta}_i \sim \rho$ i.i.d., one gets $\hat{y}_n(\mathbf{x}; \mathcal{W}) \approx \hat{y}(\mathbf{x}; \rho)$. An intriguing observation is that, given \mathcal{L} convex in the second argument, $\mathbb{E}_{\mathcal{P}} \{\mathcal{L}(y, \hat{y}(\mathbf{x}; \rho))\}$ is convex in ρ [BRV⁺06]. As another interesting fact, [MMN18] proves that under certain regularity conditions and with \mathcal{L} being the squared loss,

$$\left| \inf_{\mathcal{W}} \mathbb{E}_{\mathcal{P}} \{\mathcal{L}(y, \hat{y}_n(\mathbf{x}; \mathcal{W}))\} - \inf_{\rho} \mathbb{E}_{\mathcal{P}} \{\mathcal{L}(y, \hat{y}(\mathbf{x}; \rho))\} \right| = O\left(\frac{1}{n}\right) \xrightarrow{n \rightarrow \infty} 0. \quad (4)$$

In short, ρ is a surrogate measure for $\text{Emp}(\{\boldsymbol{\theta}_i\}_{i \in [n]})$.

Dynamics.

Using the same idea of replacing the sum with an integral, one can use the above infinite- n representation to describe the SGD dynamics. In particular, let $\hat{\rho}_n^k = \text{Emp}(\{\boldsymbol{\theta}_i^k\}_{i \in [n]})$ the empirical distribution of neuronal weights at time k on the SGD dynamics. Suppose that given some ρ^0 , at

initialization, $\hat{\rho}_n^0 \Rightarrow \rho^0$ as $n \rightarrow \infty$. For $\alpha \downarrow 0$ as $n \rightarrow \infty$, under suitable conditions, [MMN18] shows that almost surely $\hat{\rho}_n^{\lfloor t/\alpha \rfloor}$ converges weakly to a deterministic limit ρ^t . This limit is defined via the following differential equation with random initialization:

$$\frac{d}{dt}\boldsymbol{\theta}^t = -\mathbb{E}_{\mathcal{P}} \left\{ \partial_2 \mathcal{L} \left(y, \hat{y} \left(\mathbf{x}; \rho^t \right) \right) \nabla_{\boldsymbol{\theta}} \sigma \left(\mathbf{x}; \boldsymbol{\theta}^t \right) \right\}, \quad (5)$$

where $\boldsymbol{\theta}^t \sim \rho^t$ and $\boldsymbol{\theta}^0 \sim \rho^0$. More specifically, given ρ^0 , we generate $\boldsymbol{\theta}^0 \sim \rho^0$. Then we let $\boldsymbol{\theta}^t$ evolve according to Eq. (5) from the initialization $\boldsymbol{\theta}^0$ with $\rho^t = \text{Law}(\boldsymbol{\theta}^t)$ at any time t . Note that while [MMN18] defines ρ^t via a partial differential equation, what we present here is an equivalent definition that is more convenient for our discussion.

The behavior of the network throughout the SGD dynamics thus tends to a non-trivial limit, given in an explicit formula, as the number of neurons tends to infinity. In fact, [MMN18] proves a more quantitative statement that holds so long as $n \gg d$ the data dimension and $t \leq T$ not too large.

Heuristic derivation.

A heuristic to derive Eq. (5) from Eq. (2) is by firstly, identifying $t = k\alpha$ and recognizing that $\alpha \downarrow 0$ leads to time continuum and in-expectation property w.r.t. the data, for $i \in [n]$:

$$\frac{d}{dt}\boldsymbol{\theta}_i^t \approx -\mathbb{E}_{\mathcal{P}} \left\{ \partial_2 \mathcal{L} \left(y, \hat{y}_n \left(\mathbf{x}; \mathcal{W}^t \right) \right) \nabla_{\boldsymbol{\theta}} \sigma \left(\mathbf{x}; \boldsymbol{\theta}_i^t \right) \right\}, \quad \mathcal{W}^t = \left\{ \boldsymbol{\theta}_i^t \right\}_{i \in [n]}.$$

Secondly, we again replace a sum with an integral, wherever possible. Here $\hat{y}_n(\mathbf{x}; \mathcal{W}^t) \approx \hat{y}(\mathbf{x}; \tilde{\rho}^t)$ from the statics, with $\tilde{\rho}^t$ being the surrogate measure for $\text{Emp}(\mathcal{W}^t)$ at each time $t \geq 0$, which yields

$$\frac{d}{dt}\boldsymbol{\theta}_i^t \approx -\mathbb{E}_{\mathcal{P}} \left\{ \partial_2 \mathcal{L} \left(y, \hat{y} \left(\mathbf{x}; \tilde{\rho}^t \right) \right) \nabla_{\boldsymbol{\theta}} \sigma \left(\mathbf{x}; \boldsymbol{\theta}_i^t \right) \right\}. \quad (6)$$

Thirdly, we observe symmetry among the neurons in the above. If this symmetry is attained at $t = 0$ by proper initialization, it should be maintained at all subsequent t , and hence one has $\text{Law}(\boldsymbol{\theta}_i^t) \approx \tilde{\rho}^t$ in the limit $n \rightarrow \infty$, in which case we drop the subscript i . If at initialization $\tilde{\rho}^0 = \rho^0$, then by comparing the resultant dynamics with Eq. (5), one identifies $\tilde{\rho}^t \approx \rho^t$.

1.3 Contributions

In this work, we aim to develop a formalism which describes and derives the MF limit for multilayer neural networks under suitable scalings.

From the derivation for two-layers networks, we observe that symmetry among the neurons plays a key role in the MF limit. Intuitively one may expect the same for multilayer networks in that there is symmetry among neurons of the same layer – see Fig. 3 of a three-layers network and Fig. 4 of a generic multilayer one, for visualization. Yet when one attempts to extend the argument from the two-layers case, several difficulties and questions arise:

- In the two-layers case, the network output $\hat{y}_n(\mathbf{x}; \mathcal{W})$ is a sum of signals from individual neurons which do not share weights. However in a multilayer network, neurons at layer ℓ receive signals that are constrained to come from the same set of neurons of layer $\ell - 1$ or $\ell + 1$.

- In the two-layers case, each neuron is represented by its respective weight θ_i^k at each time k . This representation is natural: $\hat{y}_n(\mathbf{x}; \mathcal{W})$ assumes the simple form of a sum, and once the approximation $\hat{y}_n(\mathbf{x}; \mathcal{W}) \approx \hat{y}(\mathbf{x}; \rho)$ is made, each neuron is updated separately under the SGD dynamics, in light of Eq. (6). However, as said above, the multilayer case presents a certain structural constraint. Moreover due to the layering structure, the update of each neuron is influenced by other neurons of the adjacent layers. In what way can we give a quantitative representation for each neuron that respects the complexity in the structure, and at the same time, exploits the neuronal symmetry to make simplifications?
- Observe that the scalings are chosen so that quantities of interests remain $O(1)$, roughly speaking. In the particular case of two-layers networks, the scaling $1/n$ in $\hat{y}_n(\mathbf{x}; \mathcal{W})$ and the factor n in the gradient update in Eq. (2) ensure that $\hat{y}_n(\mathbf{x}; \mathcal{W})$ and the differential change $(\theta_i^{k+1} - \theta_i^k)/\alpha$ are $O(1)$. Under what scalings does the MF limit behavior occur for the multilayer case?

To make a first step, we postulate that neuronal symmetry gives rise to two crucial properties, which we call *marginal uniformity* and *self-averaging*. While they are used already in the two-layers case, the complexity in a multilayer network requires more extensive and explicit use of these properties, especially self-averaging. This enables a heuristic derivation of the MF limit, revealing the answers to the aforementioned questions:

- We propose that each certain neuron is represented not directly by its corresponding weights, but by a stochastic kernel which outputs at random the corresponding weights, conditional on the neurons of the previous layer. We show how this representation, which changes from layer to layer, can adapt to the constraint of multilayer hierarchies and formalize the properties arising from neuronal symmetry.
- Despite the somewhat complex representation, interestingly to describe the MF limit of multilayer fully-connected networks, one requires only one simple statistic of the stochastic kernel: its conditional expectation. A key insight is the following: since a neuron at layer ℓ receives an aggregate of signals from a set of neurons of layer $\ell + 1$ or $\ell - 1$, this aggregate simplifies itself when one views these neurons as one whole ensemble, thanks to the self-averaging property.
- We also find that the appropriate scalings are not uniform across different layers.

We must caution the readers that our current development is non-rigorous. As such, an outstanding challenge remains: under what regularity conditions, as well as what precise mathematical sense, can the formalism hold? On the other hand, the formalism is meant to be informative: firstly, it is predictive of the MF limit behavior to be observed in real simulations when the number of neurons is sufficiently large; secondly, it explores a regime, associated with specific scalings, that is under-studied by current experimental and theoretical pursuits; thirdly, it signifies the potential for a theoretical framework to analyze and design multilayer neural networks – a quest that has recently witnessed progresses in the two-layers case.

1.4 Outline

In Section 2, we present the formalism in the particular case of a three-layers network. In particular, Section 2.1 and Section 2.2 run in parallel, each describing the forward pass, the backward pass and

the (learning or evolution) dynamics. The former section is on the neural network with scalings, and the latter is on its MF limit. We give a heuristic derivation of their connection in Section 2.3 and several remarks in Section 2.4. The case of general multilayer networks is presented in Section 3, with its heuristic derivation deferred to Appendix A. Since the treatments of these two cases are similar in spirit, the readers are urged to read Section 2, where the key ideas are explained in greater details. In Section 4, we present several experiments and a theoretical result to validate the existence of the MF limit. We particularly do not aim for achieving competitive empirical results in our experiments. It remains open to find good practices to train a network in this regime, a task that deserves another investigation.

While our main focus is fully-connected multilayer networks, the generality of the principles allows us to draw similar conclusions on certain other settings. See Appendix C where we discuss the case of multilayer convolutional neural networks.

In the following, we discuss related works.

1.5 Related works

As mentioned, several recent works have studied the MF limit in the two-layers network case. The works [MMN18, CB18b, SS18a, RVE18] establish the MF limit, and in particular, [MMN18] proves that this holds as soon as the number of neurons exceeds the data dimension. [MMN18, CB18b] utilize this limit to prove that (noisy) SGD can converge to (near) global optimum under different assumptions. For a specific class of activations and data distribution, [JMM19] proves that this convergence is exponentially fast using the displacement convexity property of the MF limit. Taking the same viewpoint, [WLLM18] proves a convergence result for a specifically chosen many-neurons limit. [RVE18, SS18b] study the fluctuations around the MF limit. Our analysis of the multilayer case requires substantial extension and new ideas, uncovering certain properties that are not obvious from the two-layers analysis (see also Section 2.4).

We take a note on the work [HJ15], which shares a few similarities with our work in the forward pass description (for instance, in Eq. (1) of [HJ15] as compared to Eq. (16) in our work). [HJ15] differs in that it takes a kernel method perspective and develops a Gaussian process formulation, which makes strong assumptions on the distribution of the weights. Its formulation does not extend beyond three layers. Meanwhile our work focuses on the MF limit, points out explicitly the appropriate scalings, proposes new crucial ideas to address the backward pass and the learning dynamics, and is not limited to any specific number of layers.

There is a vast literature on settings that assume a large number of neurons – typically specific to the over-parameterized regime. We shall mention here a recent subset. The highly non-convex nature of the optimization landscape enjoys attention from a major body of works [SS16, SC16, FB17, NH17, MBM18, NH18, VBB18, Coo18, DL18, SJJ18, YSJ19]. This is yet far from a complete picture without a study of the trajectory of the learning dynamics, which has witnessed recent progresses. Several works [LL18, DZPS19, DLL⁺18, AZLL18, AZLS18, ZCZG18] concurrently show that gradient-based learning dynamics can find the global optimum in multilayer networks, provided an extremely large number of neurons. The work [JGH18] develops a complementary viewpoint on the dynamics, the so-called neural tangent kernel, also in the limit of infinitely many neurons. A common feature of these works is that throughout the considered training period, certain properties of the network remain close to the randomized initialization, and the network behaves like kernel regression. Further discussions in this regard can be found in the recent note [CB18a]. Complementing these mathematical approaches, [GSd⁺18, SGd⁺18, GJS⁺19]

utilize the physics of jamming to make a quantitative prediction of the boundary between the over-parameterized and under-parameterized regions, as well as the generalization behavior of over-parameterized networks, under a specific choice of the loss function. In another development, several works [PLR⁺16, SGGSD17, PSG17, YS17, CPS18, XBSD⁺18, HR18, Han18, LN19, YPR⁺19] obtain good initialization strategies by studying networks with infinitely many neurons and random weights (which hence disregard the learning dynamics). These works form a basis for a Gaussian process perspective [LSdP⁺18, dGMHR⁺18, GARA19, NXB⁺19]. All these directions are not directly comparable with ours. Furthermore we note that the settings in these works assume different scalings from ours and thus do not exhibit the same MF limit behavior that is to be presented here.

2 Mean field limit in three-layers fully-connected networks

In this section, we develop a formalism in which the MF limit is derived for a three-layers neural network under suitable scalings. The focus on this specific case is made for simplicity of the presentation and illustration of the key ideas. While certain elements have already been seen in the two-layers case, there are important and substantial differences that shall be highlighted.

2.1 Setting: A three-layers network

Forward pass.

We consider the following three-layers neural network with fully-connected layers and no biases:

$$\hat{y}_n(\mathbf{x}; \mathcal{W}) = \frac{1}{n_2} \langle \boldsymbol{\beta}, \sigma(\mathbf{h}_2) \rangle, \quad \mathbf{h}_2 = \frac{1}{n_1} \mathbf{W}_2 \sigma(\mathbf{h}_1), \quad \mathbf{h}_1 = \mathbf{W}_1 \mathbf{x}, \quad (7)$$

in which $\mathbf{x} \in \mathbb{R}^d$ is the input to the network, $\hat{y}_n(\mathbf{x}; \mathcal{W}) \in \mathbb{R}$ is the output, $\mathcal{W} = \{\mathbf{W}_1, \mathbf{W}_2, \boldsymbol{\beta}\}$ is the collection of weights, $\mathbf{W}_1 \in \mathbb{R}^{n_1 \times d}$, $\mathbf{W}_2 \in \mathbb{R}^{n_2 \times n_1}$, $\boldsymbol{\beta} \in \mathbb{R}^{n_2}$, and $\sigma : \mathbb{R} \mapsto \mathbb{R}$ is a nonlinear activation. \mathbf{h}_1 and \mathbf{h}_2 are commonly called the pre-activations. Here $n_1 = n_1(n)$ and $n_2 = n_2(n)$, both of which shall be taken to ∞ as $n \rightarrow \infty$. An illustration is given in Fig. 3.(a).

Backward pass.

The backward pass computes several derivative quantities to be used for learning. Let us define:

$$\tilde{\nabla}_{\boldsymbol{\beta}} \hat{y}_n(\mathbf{x}; \mathcal{W}) = n_2 \nabla_{\boldsymbol{\beta}} \hat{y}_n(\mathbf{x}; \mathcal{W}) = \sigma(\mathbf{h}_2), \quad (8)$$

$$\tilde{\nabla}_{\mathbf{h}_2} \hat{y}_n(\mathbf{x}; \mathcal{W}) = n_2 \nabla_{\mathbf{h}_2} \hat{y}_n(\mathbf{x}; \mathcal{W}) = \boldsymbol{\beta} \odot \sigma'(\mathbf{h}_2), \quad (9)$$

$$\tilde{\nabla}_{\mathbf{W}_2} \hat{y}_n(\mathbf{x}; \mathcal{W}) = n_1 n_2 \nabla_{\mathbf{W}_2} \hat{y}_n(\mathbf{x}; \mathcal{W}) = \tilde{\nabla}_{\mathbf{h}_2} \hat{y}_n(\mathbf{x}; \mathcal{W}) \sigma(\mathbf{h}_1)^\top, \quad (10)$$

$$\tilde{\nabla}_{\mathbf{h}_1} \hat{y}_n(\mathbf{x}; \mathcal{W}) = n_1 \nabla_{\mathbf{h}_1} \hat{y}_n(\mathbf{x}; \mathcal{W}) = \frac{1}{n_2} \left(\mathbf{W}_2^\top \tilde{\nabla}_{\mathbf{h}_2} \hat{y}_n(\mathbf{x}; \mathcal{W}) \right) \odot \sigma'(\mathbf{h}_1), \quad (11)$$

$$\tilde{\nabla}_{\mathbf{W}_1} \hat{y}_n(\mathbf{x}; \mathcal{W}) = n_1 \nabla_{\mathbf{W}_1} \hat{y}_n(\mathbf{x}; \mathcal{W}) = \tilde{\nabla}_{\mathbf{h}_1} \hat{y}_n(\mathbf{x}; \mathcal{W}) \mathbf{x}^\top. \quad (12)$$

Learning dynamics.

Similar to Section 1.2, we assume that at each time $k \in \mathbb{N}$, the data $(\mathbf{x}^k, y^k) \in \mathbb{R}^d \times \mathbb{R}$ is drawn independently from a probabilistic source \mathcal{P} . We train the network with the loss $\mathcal{L}(y, \hat{y}_n(\mathbf{x}; \mathcal{W}))$

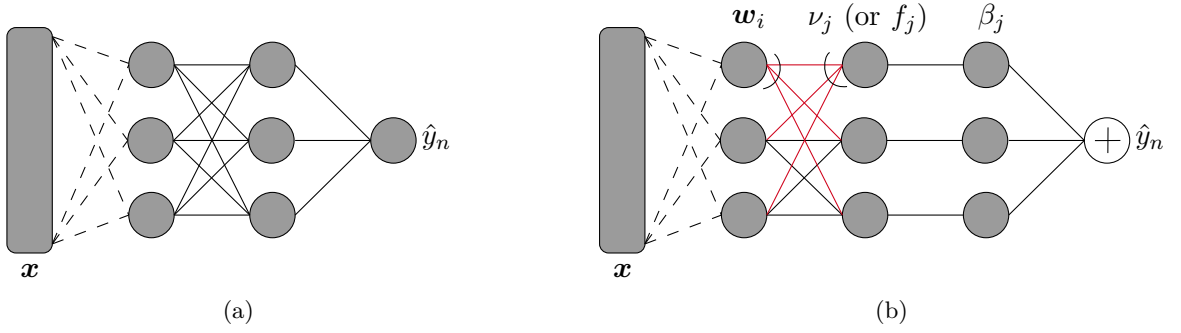


Figure 3: (a): A graphical representation of a three-layers network. (b): An equivalent representation, as proposed in Section 2.3. Neuron j of the second layer is represented by ν_j , and $f_j = \text{CE}\{\nu_j\}$. Notice that neuron j of the second layer receives the forward pass information averaged over all neurons of the first layer. Likewise, neuron i of the first layer receives the backward pass information averaged over all neurons of the second layer. However neuron j of the third layer does not average its received forward pass information over all neurons of the second layer, due to its connectivity. Likewise, neuron j of the second layer does not average its received backward pass information over all neurons of the third layer.

for a loss function $\mathcal{L} : \mathbb{R} \times \mathbb{R} \mapsto \mathbb{R}$, using SGD with an initialization $\mathcal{W}^0 = \{\mathbf{W}_1^0, \mathbf{W}_2^0, \beta^0\}$ and a learning rate $\alpha > 0$:

$$\beta^{k+1} = \beta^k - \alpha \partial_2 \mathcal{L}(y^k, \hat{y}_n(\mathbf{x}^k; \mathcal{W}^k)) \tilde{\nabla}_{\beta} \hat{y}_n(\mathbf{x}^k; \mathcal{W}^k), \quad (13)$$

$$\mathbf{W}_2^{k+1} = \mathbf{W}_2^k - \alpha \partial_2 \mathcal{L}(y^k, \hat{y}_n(\mathbf{x}^k; \mathcal{W}^k)) \tilde{\nabla}_{\mathbf{W}_2} \hat{y}_n(\mathbf{x}^k; \mathcal{W}^k), \quad (14)$$

$$\mathbf{W}_1^{k+1} = \mathbf{W}_1^k - \alpha \partial_2 \mathcal{L}(y^k, \hat{y}_n(\mathbf{x}^k; \mathcal{W}^k)) \tilde{\nabla}_{\mathbf{W}_1} \hat{y}_n(\mathbf{x}^k; \mathcal{W}^k). \quad (15)$$

This yields the learning dynamics of $\mathcal{W}^k = \{\mathbf{W}_1^k, \mathbf{W}_2^k, \beta^k\}$. Notice the scaling by n_1 , n_2 and $n_1 n_2$ at various places in Eq. (7) and Eq. (8)-(12).

2.2 Mean field limit

In the following, we describe a time-evolving system which resembles the three-layers network but does not involve the numbers of neurons n_1 and n_2 . We then state a prediction that connects this formal system with the three-layers network. This, in particular, specifies the MF limit of the three-layers network.

Forward pass.

Let us define

$$\hat{y}(\mathbf{x}; \rho_1, \rho_2) = \int \beta \sigma(H_2(f; \mathbf{x}, \rho_1)) \rho_2(df, d\beta), \quad (16)$$

where $\rho_1 \in \mathcal{P}(\mathbb{R}^d)$, $\rho_2 \in \mathcal{P}(\mathcal{F} \times \mathbb{R})$ for $\mathcal{F} = \{f : \mathbb{R}^d \mapsto \mathbb{R}\}$, and

$$H_1(\mathbf{w}; \mathbf{x}) = \langle \mathbf{w}, \mathbf{x} \rangle, \quad H_2(f; \mathbf{x}, \rho_1) = \int f(\mathbf{w}) \sigma(H_1(\mathbf{w}; \mathbf{x})) \rho_1(d\mathbf{w}).$$

This describes a system defined via ρ_1 and ρ_2 . More specifically, ρ_1 and ρ_2 are the state of the system, and the system takes $\mathbf{x} \in \mathbb{R}^d$ as input and outputs $\hat{y}(\mathbf{x}; \rho_1, \rho_2) \in \mathbb{R}$. One should compare $\hat{y}(\mathbf{x}; \rho_1, \rho_2)$, $H_1(\mathbf{w}; \mathbf{x})$ and $H_2(f; \mathbf{x}, \rho_1)$ with respectively $\hat{y}_n(\mathbf{x}; \mathcal{W})$, \mathbf{h}_1 and \mathbf{h}_2 of the three-layers network.

Backward pass.

Let us define the following quantities:

$$\Delta_\beta(f; \mathbf{x}, \rho_1) = \sigma(H_2(f; \mathbf{x}, \rho_1)), \quad (17)$$

$$\Delta_{H_2}(\beta, f; \mathbf{x}, \rho_1) = \beta \sigma'(H_2(f; \mathbf{x}, \rho_1)), \quad (18)$$

$$\Delta_{w_2}(\beta, f, \mathbf{w}; \mathbf{x}, \rho_1) = \Delta_{H_2}(\beta, f; \mathbf{x}, \rho_1) \sigma(H_1(\mathbf{w}; \mathbf{x})), \quad (19)$$

$$\Delta_{H_1}(\mathbf{w}; \mathbf{x}, \rho_1, \rho_2) = \sigma'(H_1(\mathbf{w}; \mathbf{x})) \int f(\mathbf{w}) \Delta_{H_2}(\beta, f; \mathbf{x}, \rho_1) \rho_2(d\mathbf{f}, d\beta), \quad (20)$$

$$\Delta_{w_1}(\mathbf{w}; \mathbf{x}, \rho_1, \rho_2) = \Delta_{H_1}(\mathbf{w}; \mathbf{x}, \rho_1, \rho_2) \mathbf{x}. \quad (21)$$

One should compare Eq. (17)-(21) with Eq. (8)-(12) respectively.

Evolution dynamics.

Now we describe a continuous-time evolution dynamics of the system, defined at each time t via $\rho_1^t \in \mathcal{P}(\mathbb{R}^d)$ and $\rho_2^t \in \mathcal{P}(\mathcal{F} \times \mathbb{R})$. Specifically, given $\rho_1^0 \in \mathcal{P}(\mathbb{R}^d)$ and $\rho_2^0 \in \mathcal{P}(\mathcal{F} \times \mathbb{R})$, we generate $\mathbf{w}^0 \sim \rho_1^0$ and $(f^0, \beta^0) \sim \rho_2^0$. Taking them as the initialization, we then let \mathbf{w}^t , f^t and β^t evolve according to

$$\frac{d}{dt} \mathbf{w}^t = G_w(\mathbf{w}^t; \rho_1^t, \rho_2^t), \quad (22)$$

$$\partial_t f^t(\mathbf{w}) + \langle \nabla f^t(\mathbf{w}), G_w(\mathbf{w}; \rho_1^t, \rho_2^t) \rangle = G_f(\beta^t, f^t, \mathbf{w}; \rho_1^t, \rho_2^t) \quad \forall \mathbf{w} \in \mathbb{R}^d, \quad (23)$$

$$\frac{d}{dt} \beta^t = G_\beta(f^t; \rho_1^t, \rho_2^t), \quad (24)$$

with $\rho_1^t = \text{Law}(\mathbf{w}^t)$ and $\rho_2^t = \text{Law}(f^t, \beta^t)$, where we define

$$\begin{aligned} G_w(\mathbf{w}; \rho_1, \rho_2) &= -\mathbb{E}_{\mathcal{P}} \{ \partial_2 \mathcal{L}(y, \hat{y}(\mathbf{x}; \rho_1, \rho_2)) \Delta_{w_1}(\mathbf{w}; \mathbf{x}, \rho_1, \rho_2) \}, \\ G_f(\beta, f, \mathbf{w}; \rho_1, \rho_2) &= -\mathbb{E}_{\mathcal{P}} \{ \partial_2 \mathcal{L}(y, \hat{y}(\mathbf{x}; \rho_1, \rho_2)) \Delta_{w_2}(\beta, f, \mathbf{w}; \mathbf{x}, \rho_1) \}, \\ G_\beta(f; \rho_1, \rho_2) &= -\mathbb{E}_{\mathcal{P}} \{ \partial_2 \mathcal{L}(y, \hat{y}(\mathbf{x}; \rho_1, \rho_2)) \Delta_\beta(f; \mathbf{x}, \rho_1) \}. \end{aligned}$$

The evolution is thus described by a system of partial differential equations with a random initialization.

The prediction.

We state our prediction on the connection between this system and the three-layers neural network. Given two measures $\rho_1^0 \in \mathcal{P}(\mathbb{R}^d)$ and $\rho_2^0 \in \mathcal{P}(\mathcal{F} \times \mathbb{R})$, we generate \mathbf{W}_1^0 , \mathbf{W}_2^0 and β^0 as follows. We draw the rows $\{\mathbf{w}_{1,i}^0\}_{i \in [n_1]}$ of \mathbf{W}_1^0 i.i.d. from ρ_1^0 . We also draw n_2 i.i.d. samples $\{f_j^0, \beta_j^0\}_{j \in [n_2]}$ from ρ_2^0 independently. We then form \mathbf{W}_2^0 by making $f_j^0(\mathbf{w}_{1,i}^0)$ its (j, i) -th entry. Finally we form

$\beta^0 = (\beta_1^0, \dots, \beta_{n_2}^0)^\top$. We then run the system initialized at ρ_1^0 and ρ_2^0 to obtain ρ_1^t and ρ_2^t for any t . We also train the neural network initialized at \mathbf{W}_1^0 , \mathbf{W}_2^0 and β^0 to obtain \mathcal{W}^k for any k . Our formalism states that for any $t \geq 0$, with $n \rightarrow \infty$ (and hence $n_1, n_2 \rightarrow \infty$) and $\alpha \downarrow 0$, for sufficiently regular (e.g. smooth and bounded) $\phi : \mathbb{R} \times \mathbb{R} \mapsto \mathbb{R}$,

$$\mathbb{E}_{\mathcal{P}} \left\{ \phi \left(y, \hat{y}_n \left(\mathbf{x}; \mathcal{W}^{\lfloor t/\alpha \rfloor} \right) \right) \right\} \rightarrow \mathbb{E}_{\mathcal{P}} \left\{ \phi \left(y, \hat{y} \left(\mathbf{x}; \rho_1^t, \rho_2^t \right) \right) \right\}$$

in probability over the randomness of initialization and data generation throughout SGD learning.

In fact, it is our expectation that a more general behavior could be observed. For example, we expect that for any $t \geq 0$, with $n \rightarrow \infty$ and $\alpha \downarrow 0$,

$$\mathbb{E}_{\mathcal{P}_{\text{test}}} \left\{ \phi \left(y, \hat{y}_n \left(\mathbf{x}; \mathcal{W}^{\lfloor t/\alpha \rfloor} \right) \right) \right\} \rightarrow \mathbb{E}_{\mathcal{P}_{\text{test}}} \left\{ \phi \left(y, \hat{y} \left(\mathbf{x}; \rho_1^t, \rho_2^t \right) \right) \right\}$$

in probability, where $\mathcal{P}_{\text{test}}$ is an out-of-sample distribution.

2.3 From three-layers network to the mean field limit: a heuristic derivation

To heuristically derive a connection between the three-layers network and its corresponding formal system, we first state our postulates.

The postulates.

We observe that there is symmetry in the role among the neurons of the same layer. This symmetry, once attained by proper initialization, is expected to hold at all subsequent time. This, in particular, suggests the following two properties:

- (a) **Marginal uniformity:** If a law that governs neuron i of layer ℓ depends on other neurons of layer ℓ only through global statistics of layer ℓ , then this law applies to all neurons of layer ℓ .
- (b) **Self-averaging:** One can replace a sum of sufficiently many terms, which display symmetry in their roles and each of which corresponds to one neuron from the same layer, with an appropriate integral. More explicitly, if we associate neuron i among the n neurons of the same layer with $g(x_i, A_i)$, where A_i is a random quantity sampled independently from a measure μ_i of neuron i , then for sufficiently large n ,

$$\frac{1}{n} \sum_{i=1}^n g(x_i, A_i) \approx \int g(x, a) \mu(da) \rho(dx, d\mu) \quad (25)$$

for an appropriate probability measure ρ which plays a surrogate role for the ensemble of neurons of this layer.

These properties suggest that one can obtain a non-trivial description, independent of the number of neurons, of the network as n grows large.

To quantify the above properties, it is necessary to represent each neuron with a quantity. We propose the following representation, which accords with the graphical model in Fig. 3.(b):

- At the first layer, neuron i is represented by the weight vector $\mathbf{w}_{1,i} \in \mathbb{R}^d$ (the i -th row of \mathbf{W}_1).

- At the second layer, neuron j is represented by a stochastic kernel $\nu_j \in \mathcal{K}(\mathbb{R}^d, \mathbb{R})$. Neuron j generates the weight $w_{2,ji}$ (the (j, i) -th entry of \mathbf{W}_2) according to $\nu_j(\cdot | \mathbf{w}_{1,i})$.
- At the third layer, neuron j is represented by the weight $\beta_j \in \mathbb{R}$.

Representation by the weights $\{\mathbf{w}_{1,i}\}_{i \in [n_1]}$ and $\{\beta_j\}_{j \in [n_2]}$ is natural. The crucial role of stochastic kernels $\{\nu_j\}_{j \in [n_2]}$ will be clearer later (cf. Section 2.4), even though they do not appear in the description of the formal system in Section 2.2.

We are now ready to give a heuristic derivation of the connection between the three-layers network and the formal system.

Forward pass.

Let us derive Eq. (16) from Eq. (7). Similar to the two-layers case, we have for large n_1 , at each neuron j of the second layer for $j \in [n_2]$:

$$h_{2,j} = \frac{1}{n_1} \langle \mathbf{w}_{2,j}, \sigma(\mathbf{W}_1 \mathbf{x}) \rangle \approx \int w_2 \sigma(\langle \mathbf{w}, \mathbf{x} \rangle) \nu_j(dw_2 | \mathbf{w}) \rho_1(d\mathbf{w}). \quad (26)$$

Here in the approximation, we have replaced the empirical measure $\text{Emp}(\{\mathbf{w}_{1,i}, w_{2,ji}\}_{i \in [n_1]})$ with $\nu_j \rho_1$, by the self-averaging property. We also note that unlike the two-layers case, $h_{2,j}$'s for different neuron j 's involve the same \mathbf{W}_1 of the first layer. This is reflected in the use of ρ_1 independent of j . Now by setting

$$f_j(\mathbf{w}) = \text{CE}\{\nu_j\}(\mathbf{w}) = \int w_2 \nu_j(dw_2 | \mathbf{w}), \quad (27)$$

we obtain

$$h_{2,j} \approx H_2(f_j; \mathbf{x}, \rho_1). \quad (28)$$

This results in

$$\hat{y}_n(\mathbf{x}; \mathcal{W}) = \frac{1}{n_2} \sum_{j=1}^{n_2} \beta_j \sigma(h_{2,j}) \approx \frac{1}{n_2} \sum_{j=1}^{n_2} \beta_j \sigma(H_2(f_j; \mathbf{x}, \rho_1)).$$

Applying self-averaging again, we finally obtain, for large n_2 ,

$$\hat{y}_n(\mathbf{x}; \mathcal{W}) \approx \int \beta \sigma(H_2(f; \mathbf{x}, \rho_1)) \rho_2(df, d\beta) = \hat{y}(\mathbf{x}; \rho_1, \rho_2). \quad (29)$$

From this derivation, we see that:

- ρ_1 is a surrogate measure for $\text{Emp}(\{\mathbf{w}_{1,i}\}_{i \in [n_1]})$ for the first layer's neurons;
- ρ_2 is a surrogate measure for $\text{Emp}(\{f_j, \beta_j\}_{j \in [n_2]})$ for the second and third layers' neurons;
- as per Eq. (27), the only information about ν_j that is used to compute the forward pass is f_j .

Backward pass.

We derive the respective connection between Eq. (17)-(21) and Eq. (8)-(12). From Eq. (28), we have immediately:

$$\begin{aligned} \left(\tilde{\nabla}_{\beta}\hat{y}_n(\mathbf{x};\mathcal{W})\right)_j &= \sigma(h_{2,j}) \approx \Delta_{\beta}(f_j; \mathbf{x}, \rho_1), \\ \left(\tilde{\nabla}_{h_2}\hat{y}_n(\mathbf{x};\mathcal{W})\right)_j &= \beta_j\sigma'(h_{2,j}) \approx \Delta_{H_2}(\beta_j, f_j; \mathbf{x}, \rho_1), \end{aligned} \quad (30)$$

which gives

$$\begin{aligned} \left(\tilde{\nabla}_{\mathbf{w}_2}\hat{y}_n(\mathbf{x};\mathcal{W})\right)_{ji} &= \left(\tilde{\nabla}_{h_2}\hat{y}_n(\mathbf{x};\mathcal{W})\right)_j \sigma(h_{1,i}) \\ &\approx \Delta_{H_2}(\beta_j, f_j; \mathbf{x}, \rho_1) \sigma(\langle \mathbf{w}_{1,i}, \mathbf{x} \rangle) = \Delta_{w_2}(\beta_j, f_j, \mathbf{w}_{1,i}; \mathbf{x}, \rho_1). \end{aligned} \quad (31)$$

Let us consider $\tilde{\nabla}_{h_1}\hat{y}_n(\mathbf{x};\mathcal{W})$:

$$\begin{aligned} \left(\tilde{\nabla}_{h_1}\hat{y}_n(\mathbf{x};\mathcal{W})\right)_i &= \left(\frac{1}{n_2} \sum_{j=1}^{n_2} w_{2,ji} \left(\tilde{\nabla}_{h_2}\hat{y}_n(\mathbf{x};\mathcal{W})\right)_j\right) \sigma'(h_{1,i}) \\ &\approx \left(\frac{1}{n_2} \sum_{j=1}^{n_2} w_{2,ji} \Delta_{H_2}(\beta_j, f_j; \mathbf{x}, \rho_1)\right) \sigma'(\langle \mathbf{w}_{1,i}, \mathbf{x} \rangle). \end{aligned}$$

Recall that $f_j = \text{CE}\{\nu_j\}$. By our proposed representation, given a fixed $\mathbf{w}_{1,i}$ we have $w_{2,ji} \sim \nu_j(\cdot|\mathbf{w}_{1,i})$. Hence we can again apply self-averaging in the following way:

$$\begin{aligned} \frac{1}{n_2} \sum_{j=1}^{n_2} w_{2,ji} \Delta_{H_2}(\beta_j, f_j; \mathbf{x}, \rho_1) &\approx \int w_2 \Delta_{H_2}(\beta, \text{CE}\{\nu\}; \mathbf{x}, \rho_1) \nu(dw_2|\mathbf{w}_{1,i}) \mu(d\nu, d\beta) \\ &= \int \text{CE}\{\nu\}(\mathbf{w}_{1,i}) \Delta_{H_2}(\beta, \text{CE}\{\nu\}; \mathbf{x}, \rho_1) \mu(d\nu, d\beta), \end{aligned} \quad (32)$$

for a probability measure μ surrogate for $\text{Emp}\left(\{\nu_j, \beta_j\}_{j \in [n_2]}\right)$. We make further simplification by observing that the integrand depends on ν only through $\text{CE}\{\nu\}$ and recalling that ρ_2 is the surrogate measure for $\text{Emp}\left(\{f_j, \beta_j\}_{j \in [n_2]}\right)$:

$$\left(\tilde{\nabla}_{h_1}\hat{y}_n(\mathbf{x};\mathcal{W})\right)_i \approx \left(\int f(\mathbf{w}_{1,i}) \Delta_{H_2}(\beta, f; \mathbf{x}, \rho_1) \rho_2(df, d\beta)\right) \sigma'(\langle \mathbf{w}_{1,i}, \mathbf{x} \rangle) = \Delta_{H_1}(\mathbf{w}_{1,i}; \mathbf{x}, \rho_1, \rho_2).$$

Finally we consider the i -th row of $\tilde{\nabla}_{\mathbf{w}_1}\hat{y}_n(\mathbf{x};\mathcal{W})$:

$$\left(\tilde{\nabla}_{\mathbf{w}_1}\hat{y}_n(\mathbf{x};\mathcal{W})\right)_i = \left(\tilde{\nabla}_{h_1}\hat{y}_n(\mathbf{x};\mathcal{W})\right)_i \mathbf{x} \approx \Delta_{H_1}(\mathbf{w}_{1,i}; \mathbf{x}, \rho_1, \rho_2) \mathbf{x} = \Delta_{\mathbf{w}_1}(\mathbf{w}_{1,i}; \mathbf{x}, \rho_1, \rho_2). \quad (33)$$

We observe that like the forward pass, the only information about ν_j that is used to compute the backward pass is f_j .

Learning dynamics.

We derive the evolution dynamics (22)-(24) of the formal system from the SGD dynamics (13)-(15) of the neural network. First, by identifying $t = k\alpha$ and taking $\alpha \downarrow 0$, one obtains time continuum and in-expectation property w.r.t. \mathcal{P} from the SGD dynamics:

$$\begin{aligned}\frac{d}{dt}\beta^t &= -\mathbb{E}_{\mathcal{P}} \left\{ \partial_2 \mathcal{L} \left(y, \hat{y}_n \left(\mathbf{x}; \mathcal{W}^t \right) \right) \tilde{\nabla}_{\beta} \hat{y}_n \left(\mathbf{x}; \mathcal{W}^t \right) \right\}, \\ \frac{d}{dt} \mathbf{W}_2^t &= -\mathbb{E}_{\mathcal{P}} \left\{ \partial_2 \mathcal{L} \left(y, \hat{y}_n \left(\mathbf{x}; \mathcal{W}^t \right) \right) \tilde{\nabla}_{\mathbf{W}_2} \hat{y}_n \left(\mathbf{x}; \mathcal{W}^t \right) \right\}, \\ \frac{d}{dt} \mathbf{W}_1^t &= -\mathbb{E}_{\mathcal{P}} \left\{ \partial_2 \mathcal{L} \left(y, \hat{y}_n \left(\mathbf{x}; \mathcal{W}^t \right) \right) \tilde{\nabla}_{\mathbf{W}_1} \hat{y}_n \left(\mathbf{x}; \mathcal{W}^t \right) \right\},\end{aligned}$$

in which $\mathcal{W}^t = \{\mathbf{W}_1^t, \mathbf{W}_2^t, \beta^t\}$. We represent the neurons, at time t , by $\{\mathbf{w}_{1,i}^t\}_{i \in [n_1]}$, $\{\nu_j^t\}_{j \in [n_2]}$ and $\{\beta_j^t\}_{j \in [n_2]}$, in which $\mathbf{w}_{1,i}^t$ is the i -th row of \mathbf{W}_1^t , β_j^t is the j -th entry of β^t , $\nu_j^t \in \mathcal{K}(\mathbb{R}^d, \mathbb{R})$ and the (j, i) -th entry of \mathbf{W}_2^t being $w_{2,ji}^t \sim \nu_j^t(\cdot | \mathbf{w}_{1,i}^t)$. We also define $f_j^t = \text{CE}\{\nu_j^t\}$.

From Eq. (29), (30), (31) and (33), letting $\tilde{\rho}_1^t$ and $\tilde{\rho}_2^t$ be surrogate measures for respectively $\text{Emp}\left(\left\{\mathbf{w}_{1,i}^t\right\}_{i \in [n_1]}\right)$ and $\text{Emp}\left(\left\{f_j^t, \beta_j^t\right\}_{j \in [n_2]}\right)$, it is easy to see that at any time $t \geq 0$, for $j \in [n_2]$ and $i \in [n_1]$,

$$\frac{d}{dt} \beta_j^t \approx G_{\beta} \left(f_j^t; \tilde{\rho}_1^t, \tilde{\rho}_2^t \right), \quad (34)$$

$$\frac{d}{dt} w_{2,ji}^t \approx G_f \left(\beta_j^t, f_j^t, \mathbf{w}_{1,i}^t; \tilde{\rho}_1^t, \tilde{\rho}_2^t \right), \quad (35)$$

$$\frac{d}{dt} \mathbf{w}_{1,i}^t \approx G_w \left(\mathbf{w}_{1,i}^t; \tilde{\rho}_1^t, \tilde{\rho}_2^t \right). \quad (36)$$

Recall that $w_{2,ji}^t \sim \nu_j^t(\cdot | \mathbf{w}_{1,i}^t)$. A key observation is that the right-hand side of Eq. (35) does not depend on $w_{2,ji}^t$. As such, for $\Delta t \rightarrow 0$ and any event $E \subseteq \mathbb{R}$,

$$\nu_j^{t+\Delta t} \left(E + G_f \left(\beta_j^t, f_j^t, \mathbf{w}_{1,i}^t; \tilde{\rho}_1^t, \tilde{\rho}_2^t \right) \Delta t \middle| \mathbf{w}_{1,i}^{t+\Delta t} \right) \approx \nu_j^t \left(E \middle| \mathbf{w}_{1,i}^t \right).$$

We then get:

$$\begin{aligned}\frac{d}{dt} \left(f_j^t \left(\mathbf{w}_{1,i}^t \right) \right) &= \lim_{\Delta t \rightarrow 0} \frac{1}{\Delta t} \left(\int w_2 \nu_j^{t+\Delta t} \left(dw_2 \middle| \mathbf{w}_{1,i}^{t+\Delta t} \right) - \int w_2 \nu_j^t \left(dw_2 \middle| \mathbf{w}_{1,i}^t \right) \right) \\ &\approx \lim_{\Delta t \rightarrow 0} \frac{1}{\Delta t} \left(\int \left(w_2 + G_f \left(\beta_j^t, f_j^t, \mathbf{w}_{1,i}^t; \tilde{\rho}_1^t, \tilde{\rho}_2^t \right) \Delta t \right) \nu_j^t \left(dw_2 \middle| \mathbf{w}_{1,i}^t \right) - \int w_2 \nu_j^t \left(dw_2 \middle| \mathbf{w}_{1,i}^t \right) \right) \\ &= G_f \left(\beta_j^t, f_j^t, \mathbf{w}_{1,i}^t; \tilde{\rho}_1^t, \tilde{\rho}_2^t \right).\end{aligned}$$

On the other hand,

$$\begin{aligned}\frac{d}{dt} \left(f_j^t \left(\mathbf{w}_{1,i}^t \right) \right) &= \left(\partial_t f_j^t \right) \left(\mathbf{w}_{1,i}^t \right) + \left\langle \nabla f_j^t \left(\mathbf{w}_{1,i}^t \right), \frac{d}{dt} \mathbf{w}_{1,i}^t \right\rangle \\ &\approx \left(\partial_t f_j^t \right) \left(\mathbf{w}_{1,i}^t \right) + \left\langle \nabla f_j^t \left(\mathbf{w}_{1,i}^t \right), G_w \left(\mathbf{w}_{1,i}^t; \tilde{\rho}_1^t, \tilde{\rho}_2^t \right) \right\rangle,\end{aligned}$$

by Eq. (36). Hence,

$$\left(\partial_t f_j^t\right)\left(\mathbf{w}_{1,i}^t\right)+\left\langle\nabla f_j^t\left(\mathbf{w}_{1,i}^t\right), G_{\mathbf{w}}\left(\mathbf{w}_{1,i}^t ; \tilde{\rho}_1^t, \tilde{\rho}_2^t\right)\right\rangle \approx G_f\left(\beta_j^t, f_j^t, \mathbf{w}_{1,i}^t ; \tilde{\rho}_1^t, \tilde{\rho}_2^t\right) .$$

The marginal uniformity property applied to Eq. (36) posits that $\text{Law}\left(\mathbf{w}_{1,i}^t\right)$ is independent of i , and the self-averaging property then suggests $\text{Law}\left(\mathbf{w}_{1,i}^t\right) \approx \tilde{\rho}_1^t$ in the limit $n \rightarrow \infty$. In this case we also have

$$\left(\partial_t f_j^t\right)(\mathbf{w})+\left\langle\nabla f_j^t(\mathbf{w}), G_{\mathbf{w}}\left(\mathbf{w} ; \tilde{\rho}_1^t, \tilde{\rho}_2^t\right)\right\rangle \approx G_f\left(\beta_j^t, f_j^t, \mathbf{w} ; \tilde{\rho}_1^t, \tilde{\rho}_2^t\right) \quad (37)$$

for $\tilde{\rho}_1^t$ -a.e. \mathbf{w} . Observe that at any time t , values of f_j^t at $\mathbf{w} \notin \text{supp}\left(\tilde{\rho}_1^t\right)$ are used in the computation of neither the forward pass nor the backward pass. As such, we can extend the dynamic (37) to all $\mathbf{w} \in \mathbb{R}^d$ without affecting the prediction stated in Section 2.2. Applying again marginal uniformity and self-averaging to Eq. (34) and (37), we have $\text{Law}\left(f_j^t, \beta_j^t\right) \approx \tilde{\rho}_2^t$ independent of j in the limit $n \rightarrow \infty$. If $\tilde{\rho}_1^0 = \rho_1^0$ and $\tilde{\rho}_2^0 = \rho_2^0$ then one identifies $\tilde{\rho}_1^t \approx \rho_1^t$ and $\tilde{\rho}_2^t \approx \rho_2^t$. This completes the derivation.

Finally we note that the initialization in the prediction statement in Section 2.2 is sufficient to ensure firstly that symmetry among the neurons is attained at initialization and hence at all subsequent time, and secondly $\tilde{\rho}_1^0 = \rho_1^0$ and $\tilde{\rho}_2^0 = \rho_2^0$.

2.4 Discussions

Having established the MF limit and its derivation, we now make several discussions. These discussions extend in a similar spirit to the case of general multilayer networks.

Comparison with the two-layers case. We remark on two differences, which are not apparent from the last sections, in the formulations between the two-layers case and the three-layers (or multilayer) case:

- In the two-layers case, the population loss $\mathbb{E}_{\mathcal{P}}\left\{\mathcal{L}\left(y, \hat{y}\left(\mathbf{x} ; \rho\right)\right)\right\}$ is convex in ρ , if \mathcal{L} is convex in the second argument. In the three-layers case, the many-neurons description $\hat{y}\left(\mathbf{x} ; \rho_1, \rho_2\right)$ as per Eq. (16) is no longer linear in $\left(\rho_1, \rho_2\right)$ and hence $\mathbb{E}_{\mathcal{P}}\left\{\mathcal{L}\left(y, \hat{y}\left(\mathbf{x} ; \rho_1, \rho_2\right)\right)\right\}$ is generally non-convex in $\left(\rho_1, \rho_2\right)$ (although it is convex in ρ_2). This highlights the complexity of multilayer structures.
- In the two-layers case, in both the forward and backward passes, self-averaging is used only at the output $\hat{y}_n\left(\mathbf{x} ; \mathcal{W}\right) \approx \hat{y}\left(\mathbf{x} ; \rho\right)$. In the three-layers case, self-averaging occurs not only at the output but also at certain neurons, which is evident from Eq. (26) and (32).

Occurrences of self-averaging can be spotted visually from the connectivity among layers. Compare Fig. 3.(b) (or Fig. 4) against Fig. 2.(b) for visualization. Except for the connection between the last layer and the second last one, all other pairs of adjacent layers are densely connected. Also notice that the last layer's connectivity is similar to that of a two-layers network. For a neuron at layer ℓ , self-averaging occurs in the forward pass information it receives from layer $\ell-1$, if layer ℓ is not the last layer, provided that this piece of information assumes the form (25). Likewise, self-averaging occurs in the backward pass information it receives from layer $\ell+1$, if layer $\ell+1$ is not the last layer, provided that this piece of information assumes the form (25).

Stochastic kernel representation. We remark on the use of stochastic kernels $\{\nu_j\}_{j \in [n_2]}$. On one hand, given any \mathbf{W}_1 , any \mathbf{W}_2 can be realized by means of the random generation $w_{2,ji} \sim \nu_j(\cdot | \mathbf{w}_{1,i})$ for suitable $\{\nu_j\}_{j \in [n_2]}$. On the other hand, this random generation enables the application of self-averaging to make the approximation (32), which is a crucial step in the backward pass analysis.

The scalings. We comment on the rationale behind the scalings by the numbers of neurons n_1 and n_2 in the three-layers network (7) and its gradient update quantities (8)-(12). The principle is, roughly speaking, to maintain each entry in the pre-activations \mathbf{h}_1 and \mathbf{h}_2 , the output $\hat{y}_n(\mathbf{x}; \mathcal{W})$, as well as their iteration-to-iteration changes, to be $O(1)$. It is done by a simple practice: we normalize any quantity which is a sum over neurons of the same layer by its number of neurons in both the forward and backward passes. This effectively enables self-averaging in light of Eq. (25).

A consequence of this principle is that while the gradient update of \mathbf{W}_1 has a factor of n_1 similar to the two-layers case (recalling Eq. (12) and Eq. (2)), that of \mathbf{W}_2 is $n_1 n_2$ as per Eq. (10). In general, for multilayer networks, the gradient update of a weight matrix that is not of the first layer is scaled by its total number of entries. Furthermore, each entry of \mathbf{W}_2 (or any weight matrices, not of the first layer, in the multilayer case) remains $O(1)$, distinct from \mathbf{W}_1 whose rows must adapt to \mathbf{x} and whose entries are therefore not necessarily $O(1)$.

On the learning rule. While we have used a fixed learning rate for simplicity of presentation, the formalism can easily incorporate a non-uniform varying learning rate schedule. Specifically if we modify the SGD updates (13)-(15) as follows:

$$\begin{aligned}\beta^{k+1} &= \beta^k - \alpha \xi_0(k\alpha) \partial_2 \mathcal{L}(y^k, \hat{y}_n(\mathbf{x}^k; \mathcal{W}^k)) \tilde{\nabla}_{\beta} \hat{y}_n(\mathbf{x}^k; \mathcal{W}^k), \\ \mathbf{W}_2^{k+1} &= \mathbf{W}_2^k - \alpha \xi_2(k\alpha) \partial_2 \mathcal{L}(y^k, \hat{y}_n(\mathbf{x}^k; \mathcal{W}^k)) \tilde{\nabla}_{\mathbf{W}_2} \hat{y}_n(\mathbf{x}^k; \mathcal{W}^k), \\ \mathbf{W}_1^{k+1} &= \mathbf{W}_1^k - \alpha \xi_1(k\alpha) \partial_2 \mathcal{L}(y^k, \hat{y}_n(\mathbf{x}^k; \mathcal{W}^k)) \tilde{\nabla}_{\mathbf{W}_1} \hat{y}_n(\mathbf{x}^k; \mathcal{W}^k),\end{aligned}$$

for sufficiently regular functions ξ_0 , ξ_1 and ξ_2 , then the evolution dynamics of the formal system (22)-(24) should be adjusted to:

$$\begin{aligned}\frac{d}{dt} \mathbf{w}^t &= \xi_1(t) G_{\mathbf{w}}(\mathbf{w}^t; \rho_1^t, \rho_2^t), \\ \partial_t f^t(\mathbf{w}) + \langle \nabla f^t(\mathbf{w}), G_{\mathbf{w}}(\mathbf{w}; \rho_1^t, \rho_2^t) \rangle &= \xi_2(t) G_f(\beta^t, f^t, \mathbf{w}; \rho_1^t, \rho_2^t) \quad \forall \mathbf{w} \in \mathbb{R}^d, \\ \frac{d}{dt} \beta^t &= \xi_0(t) G_{\beta}(f^t; \rho_1^t, \rho_2^t).\end{aligned}$$

The same prediction holds as we take $\alpha \downarrow 0$.

Non-fully-connected structures. While we have focused entirely on fully-connected networks, we expect the same principle is applicable to other types of structure that maintain the same key features. In Appendix C, we give a brief argument, as well as an experiment, to justify that this is indeed the case for one example of interest: multilayer convolutional neural networks (CNNs).

On the local operation. One key structure that is exploited here is the summation of the form (25), which does not explicitly requires a specific form of local interaction between a weight entry and the pre-activation of a neuron. Here we are interested in more general local interactions. For example, recalling the three-layers network (7), we consider the following form of the pre-activation $h_{2,j}$ of neuron j of the second layer:

$$h_{2,j} = \frac{1}{n_1} \sum_{i=1}^{n_1} \sigma^*(w_{2,ji}, h_{1,i}), \quad \sigma^* : \mathbb{R} \times \mathbb{R} \mapsto \mathbb{R}.$$

The local operation σ^* reduces to the considered three-layers case if we set $\sigma^*(w, h) = w\sigma(h)$. Since the summation structure is retained, we expect that the choice of σ^* does not play a very critical role: for a general σ^* , under the introduced scalings, the MF limit behavior can still be observed. This is demonstrated for the case of CNNs in Appendix C.

3 Mean field limit in multilayer fully-connected networks

The development in this section is parallel to Section 2.2. We describe the multilayer neural network, as well as its corresponding formal system and the prediction. This, in particular, specifies the MF limit of the network. We defer to Appendix A to give a heuristic derivation.

3.1 Setting: Multilayer fully-connected networks

Forward pass.

We describe a neural network with L hidden layers, for a given $L \geq 1$, a collection of integers $\{d, n_1, n_2, \dots, n_L\}$ and an integer $q \geq 1$:

$$\begin{aligned} \hat{y}_n(\mathbf{x}; \mathcal{W}) &= \frac{1}{n_L} \sum_{i=1}^{n_L} (\sigma_L(\Theta_L, \mathbf{h}_L))_i, \\ \mathbf{h}_\ell &= \frac{1}{n_{\ell-1}} \mathbf{W}_\ell \sigma_{\ell-1}(\Theta_{\ell-1}, \mathbf{h}_{\ell-1}), \quad \ell = 2, \dots, L, \\ \mathbf{h}_1 &= \mathbf{W}_1 \mathbf{x}, \end{aligned} \tag{38}$$

in which $\mathbf{x} \in \mathbb{R}^d$ is the input to the network, $\hat{y}_n(\mathbf{x}; \mathcal{W}) \in \mathbb{R}$ is the output, $\mathcal{W} = \{\mathbf{W}_1, \dots, \mathbf{W}_L, \Theta_1, \dots, \Theta_L\}$ is the collection of weights, $\mathbf{W}_1 \in \mathbb{R}^{n_1 \times d}$, $\mathbf{W}_\ell \in \mathbb{R}^{n_\ell \times n_{\ell-1}}$, $\Theta_\ell \in (\mathbb{R}^q)^{n_\ell}$, and $\sigma_\ell : \mathbb{R}^q \times \mathbb{R} \mapsto \mathbb{R}$ is a nonlinear activation. (We treat Θ_ℓ as a vector of length n_ℓ with each entry being an element in \mathbb{R}^q .) Here $n_\ell = n_\ell(n) \rightarrow \infty$ as $n \rightarrow \infty$. It is a common practice to use $q = 3$, $\sigma_L(\theta, h) = \theta_1 \sigma(h + \theta_2) + \theta_3$ and $\sigma_\ell(\theta, h) = \sigma(h + \theta_1)$ for $\ell < L$ and some scalar nonlinearity σ , in which case we obtain the usual $(L + 1)$ -layers fully-connected network with biases. An illustration is given in Fig. 4.

Backward pass.

Let us define the following derivative quantities:

$$\begin{aligned} \tilde{\nabla}_{\Theta_L} \hat{y}_n(\mathbf{x}; \mathcal{W}) &= n_L \nabla_{\Theta_L} \hat{y}_n(\mathbf{x}; \mathcal{W}) = \nabla_1 \sigma_L(\Theta_L, \mathbf{h}_L), \\ \tilde{\nabla}_{\mathbf{h}_L} \hat{y}_n(\mathbf{x}; \mathcal{W}) &= n_L \nabla_{\mathbf{h}_L} \hat{y}_n(\mathbf{x}; \mathcal{W}) = \partial_2 \sigma_L(\Theta_L, \mathbf{h}_L), \end{aligned}$$

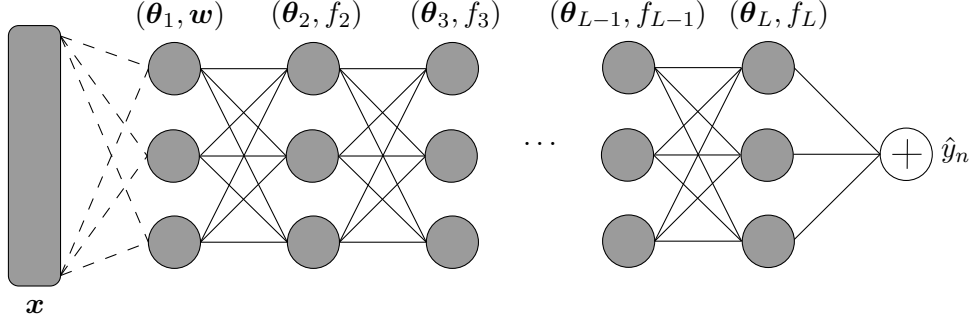


Figure 4: A graphical representation of a multilayer neural network, with $L + 1$ fully-connected layers. Here neuron j at layer $\ell > 1$ is represented by $(\boldsymbol{\theta}_{\ell,j}, f_{\ell,j})$ to be consistent with the information presented in Section 3, while we note the actual representation is $(\boldsymbol{\theta}_{\ell,j}, \nu_{\ell,j})$ for some stochastic kernel $\nu_{\ell,j}$ and $f_{\ell,j} = \text{CE}\{\nu_{\ell,j}\}$, as per the derivation in Appendix A.

$$\begin{aligned}\tilde{\nabla}_{\boldsymbol{\Theta}_\ell} \hat{y}_n(\mathbf{x}; \mathcal{W}) &= n_\ell \nabla_{\boldsymbol{\Theta}_\ell} \hat{y}_n(\mathbf{x}; \mathcal{W}) = \left(\frac{1}{n_{\ell+1}} \mathbf{W}_{\ell+1}^\top \tilde{\nabla}_{\mathbf{h}_{\ell+1}} \hat{y}_n(\mathbf{x}; \mathcal{W}) \right) \odot \nabla_1 \sigma_\ell(\boldsymbol{\Theta}_\ell, \mathbf{h}_\ell), \\ \tilde{\nabla}_{\mathbf{h}_\ell} \hat{y}_n(\mathbf{x}; \mathcal{W}) &= n_\ell \nabla_{\mathbf{h}_\ell} \hat{y}_n(\mathbf{x}; \mathcal{W}) = \left(\frac{1}{n_{\ell+1}} \mathbf{W}_{\ell+1}^\top \tilde{\nabla}_{\mathbf{h}_{\ell+1}} \hat{y}_n(\mathbf{x}; \mathcal{W}) \right) \odot \partial_2 \sigma_\ell(\boldsymbol{\Theta}_\ell, \mathbf{h}_\ell), \quad \ell = L-1, \dots, 1, \\ \tilde{\nabla}_{\mathbf{W}_\ell} \hat{y}_n(\mathbf{x}; \mathcal{W}) &= n_\ell n_{\ell-1} \nabla_{\mathbf{W}_\ell} \hat{y}_n(\mathbf{x}; \mathcal{W}) = \left(\tilde{\nabla}_{\mathbf{h}_\ell} \hat{y}_n(\mathbf{x}; \mathcal{W}) \right) \sigma_{\ell-1}(\boldsymbol{\Theta}_{\ell-1}, \mathbf{h}_{\ell-1})^\top, \quad \ell = L, \dots, 2, \\ \tilde{\nabla}_{\mathbf{W}_1} \hat{y}_n(\mathbf{x}; \mathcal{W}) &= n_1 \nabla_{\mathbf{W}_1} \hat{y}_n(\mathbf{x}; \mathcal{W}) = \left(\tilde{\nabla}_{\mathbf{h}_1} \hat{y}_n(\mathbf{x}; \mathcal{W}) \right) \mathbf{x}^\top.\end{aligned}$$

Notice the scalings by n_ℓ and $n_\ell n_{\ell-1}$.

Learning dynamics.

We assume that at each time $k \in \mathbb{N}$, the data $(\mathbf{x}^k, y^k) \in \mathbb{R}^d \times \mathbb{R}$ is drawn independently from a probabilistic source \mathcal{P} . We train the network with the loss $\mathcal{L}(y, \hat{y}_n(\mathbf{x}; \mathcal{W}))$ for a loss function $\mathcal{L} : \mathbb{R} \times \mathbb{R} \mapsto \mathbb{R}$, using SGD with an initialization $\mathcal{W}^0 = \{\mathbf{W}_1^0, \dots, \mathbf{W}_L^0, \boldsymbol{\Theta}_1^0, \dots, \boldsymbol{\Theta}_L^0\}$ and a learning rate $\alpha > 0$:

$$\begin{aligned}\mathbf{W}_\ell^{k+1} &= \mathbf{W}_\ell^k - \alpha \partial_2 \mathcal{L}(y^k, \hat{y}_n(\mathbf{x}^k; \mathcal{W}^k)) \tilde{\nabla}_{\mathbf{W}_\ell} \hat{y}_n(\mathbf{x}^k; \mathcal{W}^k), \quad \ell = 1, \dots, L, \\ \boldsymbol{\Theta}_\ell^{k+1} &= \boldsymbol{\Theta}_\ell^k - \alpha \partial_2 \mathcal{L}(y^k, \hat{y}_n(\mathbf{x}^k; \mathcal{W}^k)) \tilde{\nabla}_{\boldsymbol{\Theta}_\ell} \hat{y}_n(\mathbf{x}^k; \mathcal{W}^k), \quad \ell = 1, \dots, L.\end{aligned}$$

This yields the dynamics of $\mathcal{W}^k = \{\mathbf{W}_1^k, \dots, \mathbf{W}_L^k, \boldsymbol{\Theta}_1^k, \dots, \boldsymbol{\Theta}_L^k\}$.

3.2 Mean field limit

Similar to Section 2.2, we describe a time-evolving system which does not involve the numbers of neurons n_1, \dots, n_L . This leads to a MF limit which characterizes the behavior of the multilayer network (38) during learning in the limit $n \rightarrow \infty$ via this formal system. Before all, let $\mathcal{F}_1 = \mathbb{R}^d$ and $\mathcal{F}_\ell = \{f | f : \mathbb{R}^q \times \mathcal{F}_{\ell-1} \mapsto \mathbb{R}\}$ a vector space for $\ell = 2, \dots, L$.

Forward pass.

The forward pass of the formal system is defined by the following:

$$\hat{y}(\mathbf{x}; \underline{\rho}) = \int \sigma_L \left(\boldsymbol{\theta}, H_L \left(f; \mathbf{x}, \{\rho_i\}_{i=1}^{L-1} \right) \right) \rho_L(d\boldsymbol{\theta}, df), \quad (39)$$

where we define inductively:

$$\begin{aligned} H_1(\mathbf{w}; \mathbf{x}) &= \langle \mathbf{w}, \mathbf{x} \rangle, \\ H_2(f; \mathbf{x}, \rho_1) &= \int f(\boldsymbol{\theta}, \mathbf{w}) \sigma_1(\boldsymbol{\theta}, H_1(\mathbf{w}; \mathbf{x})) \rho_1(d\boldsymbol{\theta}, d\mathbf{w}), \\ H_\ell(f; \mathbf{x}, \{\rho_i\}_{i=1}^{\ell-1}) &= \int f(\boldsymbol{\theta}, g) \sigma_{\ell-1} \left(\boldsymbol{\theta}, H_{\ell-1} \left(g; \mathbf{x}, \{\rho_i\}_{i=1}^{\ell-2} \right) \right) \rho_{\ell-1}(d\boldsymbol{\theta}, dg), \quad \ell = 3, \dots, L, \end{aligned}$$

for which $\underline{\rho} = \{\rho_i\}_{i=1}^L$, $\rho_\ell \in \mathcal{P}(\mathbb{R}^q \times \mathcal{F}_\ell)$ for $\ell = 1, \dots, L-1$. Specifically, $\underline{\rho}$ is the state of the system, and the system takes $\mathbf{x} \in \mathbb{R}^d$ as input and outputs $\hat{y}(\mathbf{x}; \underline{\rho}) \in \mathbb{R}$. One should compare Eq. (39) with the multilayer network (38).

Backward pass.

We define the quantities $\Delta_{\boldsymbol{\theta}, \ell}$ and $\Delta_{H, \ell}$ for $\ell = 1, \dots, L$ as follows. First we define the quantities for $\ell = L$:

$$\begin{aligned} \Delta_{\boldsymbol{\theta}, L}(\boldsymbol{\theta}, f; \mathbf{x}, \{\rho_i\}_{i=1}^{L-1}) &= \nabla_1 \sigma_L \left(\boldsymbol{\theta}, H_L \left(f; \mathbf{x}, \{\rho_i\}_{i=1}^{L-1} \right) \right), \\ \Delta_{H, L}(\boldsymbol{\theta}, f; \mathbf{x}, \{\rho_i\}_{i=1}^{L-1}) &= \partial_2 \sigma_L \left(\boldsymbol{\theta}, H_L \left(f; \mathbf{x}, \{\rho_i\}_{i=1}^{L-1} \right) \right). \end{aligned}$$

Then we define the rest inductively:

$$\begin{aligned} \Delta_{\boldsymbol{\theta}, L-1}(\boldsymbol{\theta}, f; \mathbf{x}, \underline{\rho}) &= \left(\int g(\boldsymbol{\theta}, f) \Delta_{H, L}(\boldsymbol{\theta}', g; \mathbf{x}, \{\rho_i\}_{i=1}^{L-1}) \rho_L(d\boldsymbol{\theta}', dg) \right) \nabla_1 \sigma_{L-1} \left(\boldsymbol{\theta}, H_{L-1} \left(f; \mathbf{x}, \{\rho_i\}_{i=1}^{L-2} \right) \right), \\ \Delta_{H, L-1}(\boldsymbol{\theta}, f; \mathbf{x}, \underline{\rho}) &= \left(\int g(\boldsymbol{\theta}, f) \Delta_{H, L}(\boldsymbol{\theta}', g; \mathbf{x}, \{\rho_i\}_{i=1}^{L-1}) \rho_L(d\boldsymbol{\theta}', dg) \right) \partial_2 \sigma_{L-1} \left(\boldsymbol{\theta}, H_{L-1} \left(f; \mathbf{x}, \{\rho_i\}_{i=1}^{L-2} \right) \right), \\ \Delta_{\boldsymbol{\theta}, \ell}(\boldsymbol{\theta}, f; \mathbf{x}, \underline{\rho}) &= \left(\int g(\boldsymbol{\theta}, f) \Delta_{H, \ell+1}(\boldsymbol{\theta}', g; \mathbf{x}, \underline{\rho}) \rho_{\ell+1}(d\boldsymbol{\theta}', dg) \right) \nabla_1 \sigma_\ell \left(\boldsymbol{\theta}, H_\ell \left(f; \mathbf{x}, \{\rho_i\}_{i=1}^{\ell-1} \right) \right), \\ \Delta_{H, \ell}(\boldsymbol{\theta}, f; \mathbf{x}, \underline{\rho}) &= \left(\int g(\boldsymbol{\theta}, f) \Delta_{H, \ell+1}(\boldsymbol{\theta}', g; \mathbf{x}, \underline{\rho}) \rho_{\ell+1}(d\boldsymbol{\theta}', dg) \right) \partial_2 \sigma_\ell \left(\boldsymbol{\theta}, H_\ell \left(f; \mathbf{x}, \{\rho_i\}_{i=1}^{\ell-1} \right) \right), \\ &\quad \ell = L-2, \dots, 2, \\ \Delta_{\boldsymbol{\theta}, 1}(\boldsymbol{\theta}, \mathbf{w}; \mathbf{x}, \underline{\rho}) &= \left(\int g(\boldsymbol{\theta}, \mathbf{w}) \Delta_{H, 2}(\boldsymbol{\theta}', g; \mathbf{x}, \underline{\rho}) \rho_2(d\boldsymbol{\theta}', dg) \right) \nabla_1 \sigma_1(\boldsymbol{\theta}, H_1(\mathbf{w}; \mathbf{x})), \\ \Delta_{H, 1}(\boldsymbol{\theta}, f; \mathbf{x}, \underline{\rho}) &= \left(\int g(\boldsymbol{\theta}, \mathbf{w}) \Delta_{H, 2}(\boldsymbol{\theta}', g; \mathbf{x}, \underline{\rho}) \rho_2(d\boldsymbol{\theta}', dg) \right) \partial_2 \sigma_1(\boldsymbol{\theta}, H_1(\mathbf{w}; \mathbf{x})). \end{aligned}$$

From these quantities, we define $\Delta_{W, \ell}$ for $\ell = 1, \dots, L$:

$$\begin{aligned} \Delta_{W, L}(\boldsymbol{\theta}, f, \boldsymbol{\theta}', g; \mathbf{x}, \{\rho_i\}_{i=1}^{L-1}) &= \Delta_{H, L}(\boldsymbol{\theta}, f; \mathbf{x}, \{\rho_i\}_{i=1}^{L-1}) \sigma_{L-1} \left(\boldsymbol{\theta}', H_{L-1} \left(g; \mathbf{x}, \{\rho_i\}_{i=1}^{L-2} \right) \right), \\ \Delta_{W, \ell}(\boldsymbol{\theta}, f, \boldsymbol{\theta}', g; \mathbf{x}, \underline{\rho}) &= \Delta_{H, \ell}(\boldsymbol{\theta}, f; \mathbf{x}, \underline{\rho}) \sigma_{\ell-1} \left(\boldsymbol{\theta}', H_{\ell-1} \left(g; \mathbf{x}, \{\rho_i\}_{i=1}^{\ell-2} \right) \right), \quad \ell = L-1, \dots, 3, \\ \Delta_{W, 2}(\boldsymbol{\theta}, f, \boldsymbol{\theta}', \mathbf{w}; \mathbf{x}, \underline{\rho}) &= \Delta_{H, 2}(\boldsymbol{\theta}, f; \mathbf{x}, \underline{\rho}) \sigma_1(\boldsymbol{\theta}', H_1(\mathbf{w}; \mathbf{x})), \\ \Delta_{W, 1}(\boldsymbol{\theta}, \mathbf{w}; \mathbf{x}, \underline{\rho}) &= \Delta_{H, 1}(\boldsymbol{\theta}, \mathbf{w}; \mathbf{x}, \underline{\rho}) \mathbf{x}. \end{aligned}$$

As a note, except for $\Delta_{W,1}$ whose range is \mathbb{R}^d and $\Delta_{\theta,\ell}$ whose range is \mathbb{R}^q for $\ell = 1, \dots, L$, all other derivative quantities map to \mathbb{R} .

Evolution dynamics.

We describe a continuous-time evolution dynamics of the system, defined at each time t via $\underline{\rho}^t = \{\rho_\ell^t\}_{\ell=1}^L$ where $\rho_\ell^t \in \mathcal{P}(\mathbb{R}^q \times \mathcal{F}_\ell)$ for $\ell = 1, \dots, L$. First we define

$$\begin{aligned} G_{\theta,1}(\boldsymbol{\theta}, \mathbf{w}; \underline{\rho}) &= -\mathbb{E}_{\mathcal{P}} \{ \partial_2 \mathcal{L}(y, \hat{y}(\mathbf{x}; \underline{\rho})) \Delta_{\theta,1}(\boldsymbol{\theta}, \mathbf{w}; \mathbf{x}, \underline{\rho}) \}, \\ G_{\theta,\ell}(\boldsymbol{\theta}, f; \underline{\rho}) &= -\mathbb{E}_{\mathcal{P}} \{ \partial_2 \mathcal{L}(y, \hat{y}(\mathbf{x}; \underline{\rho})) \Delta_{\theta,\ell}(\boldsymbol{\theta}, f; \mathbf{x}, \underline{\rho}) \}, \quad \ell = 2, \dots, L-1, \\ G_{\theta,L}(\boldsymbol{\theta}, f; \underline{\rho}) &= -\mathbb{E}_{\mathcal{P}} \left\{ \partial_2 \mathcal{L}(y, \hat{y}(\mathbf{x}; \underline{\rho})) \Delta_{\theta,L}(\boldsymbol{\theta}, f; \mathbf{x}, \{\rho_i\}_{i=1}^{L-1}) \right\}, \\ G_{W,1}(\boldsymbol{\theta}, \mathbf{w}; \underline{\rho}) &= -\mathbb{E}_{\mathcal{P}} \{ \partial_2 \mathcal{L}(y, \hat{y}(\mathbf{x}; \underline{\rho})) \Delta_{W,1}(\boldsymbol{\theta}, \mathbf{w}; \mathbf{x}, \underline{\rho}) \}, \\ G_{f,2}(\boldsymbol{\theta}, f, \boldsymbol{\theta}', \mathbf{w}; \underline{\rho}) &= -\mathbb{E}_{\mathcal{P}} \{ \partial_2 \mathcal{L}(y, \hat{y}(\mathbf{x}; \underline{\rho})) \Delta_{W,2}(\boldsymbol{\theta}, f, \boldsymbol{\theta}', \mathbf{w}; \mathbf{x}, \underline{\rho}) \}, \\ G_{f,\ell}(\boldsymbol{\theta}, f, \boldsymbol{\theta}', g; \underline{\rho}) &= -\mathbb{E}_{\mathcal{P}} \{ \partial_2 \mathcal{L}(y, \hat{y}(\mathbf{x}; \underline{\rho})) \Delta_{W,\ell}(\boldsymbol{\theta}, f, \boldsymbol{\theta}', g; \mathbf{x}, \underline{\rho}) \}, \quad \ell = 3, \dots, L-1, \\ G_{f,L}(\boldsymbol{\theta}, f, \boldsymbol{\theta}', g; \underline{\rho}) &= -\mathbb{E}_{\mathcal{P}} \left\{ \partial_2 \mathcal{L}(y, \hat{y}(\mathbf{x}; \underline{\rho})) \Delta_{W,L}(\boldsymbol{\theta}, f, \boldsymbol{\theta}', g; \mathbf{x}, \{\rho_i\}_{i=1}^{L-1}) \right\}. \end{aligned}$$

In addition, for each $\ell = 2, \dots, L-1$, we define $\mathcal{G}_\ell : \mathbb{R}^q \times \mathcal{F}_\ell \times \mathbb{R}^q \times \mathcal{F}_{\ell-1} \mapsto \mathbb{R}$ such that, inductively,

$$\begin{aligned} \mathcal{G}_2(\boldsymbol{\theta}, f, \boldsymbol{\theta}', \mathbf{w}; \underline{\rho}) &= G_{f,2}(\boldsymbol{\theta}, f, \boldsymbol{\theta}', \mathbf{w}; \underline{\rho}) - \langle \nabla_1 f(\boldsymbol{\theta}', \mathbf{w}), G_{\theta,1}(\boldsymbol{\theta}', \mathbf{w}; \underline{\rho}) \rangle - \langle \nabla_2 f(\boldsymbol{\theta}', \mathbf{w}), G_{W,1}(\boldsymbol{\theta}', \mathbf{w}; \underline{\rho}) \rangle, \\ \mathcal{G}_\ell(\boldsymbol{\theta}, f, \boldsymbol{\theta}', g; \underline{\rho}) &= G_{f,\ell}(\boldsymbol{\theta}, f, \boldsymbol{\theta}', g; \underline{\rho}) - \langle \nabla_1 f(\boldsymbol{\theta}', g), G_{\theta,\ell-1}(\boldsymbol{\theta}', g; \underline{\rho}) \rangle - \mathcal{D}_2 f\{\boldsymbol{\theta}', g\}(\mathcal{G}_{f,\ell-1}(\boldsymbol{\theta}', g, \cdot, \cdot; \underline{\rho})), \\ &\quad \ell = 3, \dots, L. \end{aligned}$$

The evolution dynamics is then defined by the following differential equations:

$$\begin{aligned} \frac{d}{dt} \mathbf{w}^t &= G_{W,1}(\boldsymbol{\theta}_1^t, \mathbf{w}^t; \underline{\rho}^t), \\ \frac{d}{dt} \boldsymbol{\theta}_1^t &= G_{\theta,1}(\boldsymbol{\theta}_1^t, \mathbf{w}^t; \underline{\rho}^t), \\ \partial_t f_2^t(\boldsymbol{\theta}, \mathbf{w}) &= \mathcal{G}_2(\boldsymbol{\theta}_2^t, f_2^t, \boldsymbol{\theta}, \mathbf{w}; \underline{\rho}^t) \quad \forall (\boldsymbol{\theta}, \mathbf{w}) \in \mathbb{R}^q \times \mathcal{F}_1, \\ \frac{d}{dt} \boldsymbol{\theta}_\ell^t &= G_{\theta,\ell}(\boldsymbol{\theta}_\ell^t, f_\ell^t; \underline{\rho}^t), \quad \ell = 2, \dots, L, \\ \partial_t f_\ell^t(\boldsymbol{\theta}, g) &= \mathcal{G}_{f,\ell}(\boldsymbol{\theta}_\ell^t, f_\ell^t, \boldsymbol{\theta}, g; \underline{\rho}^t) \quad \forall (\boldsymbol{\theta}, g) \in \mathbb{R}^q \times \mathcal{F}_{\ell-1}, \quad \ell = 3, \dots, L, \end{aligned}$$

for $(\boldsymbol{\theta}_1^t, \mathbf{w}^t) \sim \rho_1^t$, $(\boldsymbol{\theta}_\ell^t, f_\ell^t) \sim \rho_\ell^t$ for $\ell = 2, \dots, L$, and $\underline{\rho}^t = \{\rho_\ell^t\}_{\ell=1}^L$. More specifically, given $\underline{\rho}^0 = \{\rho_\ell^0\}_{\ell=1}^L$ where $\rho_\ell^0 \in \mathcal{P}(\mathbb{R}^q \times \mathcal{F}_\ell)$, we generate $(\boldsymbol{\theta}_1^0, \mathbf{w}^0) \sim \rho_1^0$ and $(\boldsymbol{\theta}_\ell^0, f_\ell^0) \sim \rho_\ell^0$ for $\ell = 2, \dots, L$.

Taking them as the initialization, we let \mathbf{w}^t , $\{\boldsymbol{\theta}_\ell^t\}_{\ell=1}^L$ and $\{f_\ell^t\}_{\ell=2}^L$ evolve according to the aforementioned differential equations, with $\rho_1^t = \text{Law}(\boldsymbol{\theta}_1^t, \mathbf{w}^t)$ and $\rho_\ell^t = \text{Law}(\boldsymbol{\theta}_\ell^t, f_\ell^t)$ for $\ell = 2, \dots, L$.

The prediction.

We state our prediction on the connection between the formal system and the multilayer neural network. First, given $\underline{\rho}^0 = \{\rho_\ell^0 : \rho_\ell^0 \in \mathcal{P}(\mathbb{R}^q \times \mathcal{F}_\ell)\}_{\ell=1}^L$, we generate $\mathcal{W}^0 = \{\mathbf{W}_1^0, \dots, \mathbf{W}_L^0, \boldsymbol{\Theta}_1^0, \dots, \boldsymbol{\Theta}_L^0\}$ for the neural network as follows. We draw $\{\boldsymbol{\theta}_{1,i}^0, \mathbf{w}_{1,i}^0\}_{i \in [n_1]}$ i.i.d. from ρ_1^0 , where $\boldsymbol{\theta}_{1,i}^0$ is the i -th

element of Θ_1^0 and $\mathbf{w}_{1,i}^0$ is the i -th row of \mathbf{W}_1^0 . We also independently draw n_ℓ i.i.d. samples $\{\theta_{\ell,j}^0, f_{\ell,j}^0\}_{j \in [n_\ell]}$ from ρ_ℓ^0 , for $\ell = 2, \dots, L$. We then form Θ_ℓ^0 by using $\theta_{\ell,i}^0$ as its i -th element. We also form \mathbf{W}_ℓ^0 by letting its (j, i) -th entry equal $f_{\ell,j}^0(\theta_{\ell-1,i}^0, f_{\ell-1,i}^0)$ if $\ell \geq 3$ and $f_{2,j}^0(\theta_{1,i}^0, \mathbf{w}_{1,i}^0)$ if $\ell = 2$.

Given the above initialization, we run the formal system initialized at ρ^0 to obtain ρ^t for any t . We also train the neural network initialized at \mathcal{W}^0 to obtain \mathcal{W}^k for any k . Our formalism states that for any $t \geq 0$, with $n \rightarrow \infty$ (and hence $n_1, \dots, n_L \rightarrow \infty$) and $\alpha \downarrow 0$, for sufficiently regular (e.g. smooth and bounded) $\phi: \mathbb{R} \times \mathbb{R} \mapsto \mathbb{R}$,

$$\mathbb{E}_{\mathcal{P}} \left\{ \phi \left(y, \hat{y}_n \left(\mathbf{x}; \mathcal{W}^{\lfloor t/\alpha \rfloor} \right) \right) \right\} \rightarrow \mathbb{E}_{\mathcal{P}} \left\{ \phi \left(y, \hat{y} \left(\mathbf{x}; \rho^t \right) \right) \right\}$$

in probability over the randomness of initialization and data generation throughout SGD learning.

Similar to the three-layers case in Section 2.2, we expect to observe a more general behavior, for example, that for any $t \geq 0$, with $n \rightarrow \infty$ and $\alpha \downarrow 0$,

$$\mathbb{E}_{\mathcal{P}_{\text{test}}} \left\{ \phi \left(y, \hat{y}_n \left(\mathbf{x}; \mathcal{W}^{\lfloor t/\alpha \rfloor} \right) \right) \right\} \rightarrow \mathbb{E}_{\mathcal{P}_{\text{test}}} \left\{ \phi \left(y, \hat{y} \left(\mathbf{x}; \rho^t \right) \right) \right\}$$

in probability, where $\mathcal{P}_{\text{test}}$ is an out-of-sample distribution.

4 Validation of the formalism

In this section, we perform validation tests on the MF limit behavior as predicted by the formalism.

4.1 Statics: a theoretical justification

As a first test, we ask whether the forward pass description of the formalism is meaningful, in particular, whether one can obtain a result similar to Eq. (4) of the two-layers case. We shall argue that it is indeed the case, in particular,

$$\lim_{n \rightarrow \infty} \inf_{\mathcal{W}} \mathbb{E}_{\mathcal{P}} \{ \mathcal{L}(y, \hat{y}_n(\mathbf{x}; \mathcal{W})) \} = \inf_{\rho} \mathbb{E}_{\mathcal{P}} \{ \mathcal{L}(y, \hat{y}(\mathbf{x}; \rho)) \}$$

under suitable conditions. Here we recall the multilayer network (38) and its formal system (39) from Section 3, and also that $n_\ell = n_\ell(n) \rightarrow \infty$ as $n \rightarrow \infty$. This establishes an asymptotic equivalence between the global optimum of the network and that of the formal system. We defer this task to Appendix B.

4.2 Dynamics: an experimental justification

We present a second test, which aims to validate the predictions as stated in Section 2.2 and Section 3.2, via experiments. In particular, we would like to verify whether the evolution curve of a multilayer network approaches some non-trivial limiting curve as its number of neurons grows large. As a reminder, our experimental settings are not tuned to attain competitive performances since it is not our goal.

4.2.1 Experimental setting

We shall mainly consider the following three supervised learning tasks:

- **Isotropic Gaussians classification:** this is an artificial 2-classes dataset, considered in [MMN18]. The data is generated as follow: $y \sim \text{Unif}(\{-1, +1\})$, and $\mathbf{x}|y \sim \mathcal{N}(0, (1 + y\Delta)^2 \mathbf{I}_d)$, for some $\Delta \in (0, 1)$. Here we choose $d = 32$ and $\Delta = 0.4$. Note that no linear classifiers can attain non-trivial performance on this problem. We use the squared loss $\mathcal{L}(y_1, y_2) = (y_1 - y_2)^2$. We measure the population loss $\mathbb{E}_{\mathcal{P}} \{\mathcal{L}(y, \hat{y}_n(\mathbf{x}; \mathcal{W}))\}$ and the classification error $\mathcal{P}(y\hat{y}_n(\mathbf{x}; \mathcal{W}) < 0)$, estimated by Monte-Carlo averaging over 10^4 samples.
- **MNIST classification:** this is the popular MNIST 10-classes dataset. We normalize all gray-scale pixels in the image to the range $[-1, +1]$. We use the cross-entropy loss \mathcal{L} , and use the whole training set of size 60×10^3 . Here $d = 28 \times 28 = 784$. We measure the loss and the classification error, averaged over 10^4 samples drawn from the training set or the test set.
- **CIFAR-10 classification:** this is the popular CIFAR-10 dataset with 10 classes. We normalize each RGB value in the image to the range $[-1, +1]$. We use the cross-entropy loss \mathcal{L} , and use the whole training set of size 50×10^3 . Here $d = 3 \times 32 \times 32 = 3072$. We measure the loss and the classification error, averaged over 10^4 samples drawn from the training set or the test set.

To further the validation, the following task is also considered:

- **CIFAR-10 classification with VGG16 features:** the setting is almost the same as the above CIFAR-10 task, except that instead of the raw CIFAR-10 images, we use the features which are computed by the convolutional layers of the VGG16 network [SZ15] pre-trained on the ImageNet dataset [RDS⁺15]. We first upscale the images to the size $128 \times 128 \times 3$, then feed them into the VGG16 network to extract the features of dimension $d = 4 \times 4 \times 512 = 8192$. Note that the VGG16 network is not under our scalings; only the networks that we train on the VGG16 features employ the scalings.

We use the usual structure (with scalings) for an $(L + 1)$ -layers network:

$$\hat{y}_n(\mathbf{x}; \mathcal{W}) = \frac{1}{n_L} \beta \sigma \left(\mathbf{b}_L + \frac{1}{n_{L-1}} \mathbf{W}_L \sigma \left(\dots \frac{1}{n_1} \mathbf{W}_2 \sigma(\mathbf{b}_1 + \mathbf{W}_1 \mathbf{x}) \right) \right) + \mathbf{b}_{L+1},$$

where the weight matrices are $\mathbf{W}_1 \in \mathbb{R}^{n_1 \times d}$ and $\mathbf{W}_\ell \in \mathbb{R}^{n_\ell \times n_{\ell-1}}$ for $\ell = 2, \dots, L$, the output weight is $\beta \in \mathbb{R}^{n_{\text{out}} \times n_L}$, the biases are $\mathbf{b}_\ell \in \mathbb{R}^{n_\ell}$ for $\ell = 1, \dots, L$ and $\mathbf{b}_{L+1} \in \mathbb{R}^{n_{\text{out}}}$, and σ is the nonlinearity. We observe that this fits into the general description (38) of multilayer networks, except for that n_{out} can be larger than 1. Here the isotropic Gaussians classification task has $n_{\text{out}} = 1$, whereas the other two tasks have $n_{\text{out}} = 10$. While strictly speaking this is not covered by our theory, it can be extended easily to $n_{\text{out}} > 1$, provided that n_{out} remains a finite constant as $n \rightarrow \infty$. We shall also restrict our experiments to uniform widths $n_1 = \dots = n_L = n$. The scalings for gradient updates can also be easily deduced from Section 3.1.

In the experiments, unless otherwise stated, we use mini-batch SGD to perform training. Note that while we develop our theory for SGD learning dynamics in Sections 2 and 3, an inspection of their derivations reveals that the batch size does not play a role in the asymptotic $n \rightarrow \infty$ and hence does not affect the MF limit. In finite-size simulations, the use of batch size larger than 1 has the advantage of smoother evolution. We shall use a batch size of 100 in our experiments.

We now make a remark on the initialization practice. As the formalism suggests, and also as discussed in Section 2.4, the entries of the weight matrices \mathbf{W}_ℓ at layer $\ell > 1$ and the output weight β should be of the order $O(1)$. Therefore, we do the following initialization:

$$\begin{aligned} (\mathbf{W}_1^0)_{ij} &\sim \mathcal{N}\left(0, \frac{\tau_1^2}{d}\right), & (\mathbf{W}_\ell^0)_{ij} &\sim \mathcal{N}\left(\mu_2, \tau_2^2\right) \text{ for } \ell = 2, \dots, L, & (\beta^0)_{ij} &\sim \mathcal{N}\left(\mu_2, \tau_2^2\right), \\ b_{\ell,i}^0 &\sim \mathcal{N}\left(\mu_3, \tau_3^2\right) \text{ for } \ell = 1, \dots, L + 1. \end{aligned}$$

This initialization is different from the usual practice, due to the introduced scalings. A quick calculation shows that this initialization may appear degenerate in the following sense: for each \mathbf{x} , in the limit $n \rightarrow \infty$, the output $\hat{y}_n(\mathbf{x}; \mathcal{W}^0)$ at initialization becomes independent of τ_2 , and if $\tau_3 = 0$, it converges to a non-random quantity, unlike the usual practice. This is not an issue, since it corresponds to a non-trivial initialization ρ^0 of the formal system. In general, we use $\mu_2 \neq 0$.

4.2.2 Experimental results

In Fig. 5, 6 and 8, we present the results for several fully-connected networks of different n and L on the three classification tasks, with σ being the rectifier linear unit (ReLU) $\sigma(u) = \max\{0, u\}$. We observe that in each plot, the curves become increasingly matching on the whole training period as n increases, even when the networks overfit in the CIFAR-10 task. We also see that the networks display highly nonlinear dynamics and attain non-trivial performances by the end of training. In particular, it is evident from the isotropic Gaussians task that the trained networks must exploit the nonlinearity of the ReLU – even though they are initialized to be completely in the linear region of the ReLU of layer $\ell > 1$. This is because otherwise the resultant classifiers would be linear and cannot attain close to zero classification error. For the other two tasks, at each layer, we count the number of non-positive pre-activation entries and average it over the test set. Our simulations similarly indicate that by the end of training, this number amounts to a significant fraction, and therefore, the networks also exploit the nonlinearity of the ReLU.

The performance on the real datasets is realistic and not trivialized by the introduced scalings. To illustrate the point, we note that the work [PSG17] reports of a 200-layers vanilla fully-connected network, which attains a test error rate of more than 45% on the CIFAR-10 dataset. This network is initialized with i.i.d. Gaussian weights of zero mean and carefully selected variance, is trained without regularization, but is not under our scalings. We contrast this with the 4-layers network with $n = 800$ in Fig. 8, which achieves a similar test error rate of about 43%.

In Fig. 5, 7 and 9, we compare the evolutions of two initializations which differ only by the choice of τ_2 , but share the same $\tau_3 = 0$. Recall that due to the way we initialize the networks, the value of τ_2 does not affect the initial values of the network output or the pre-activations in the limit $n \rightarrow \infty$. Despite this fact, we observe in Fig. 5, 7 and 9 that the two initializations yield two different trajectories. This is consistent with our formalism: each τ_2 gives rise to a different initialization ρ^0 of the formal system and hence a different evolution trajectory.

In Fig. 10, we plot the evolution for a different choice of σ : the tanh activation. In Fig. 11, we plot the evolution of 4-layers networks for the specific task of CIFAR-10 classification with VGG16 features. We still observe that the larger n , the better the curves match. The performance in Fig. 11 is also reasonable and shows an expectedly marked improvement over networks trained on raw CIFAR-10 images; for instance, by the end of training, the network with $n = 800$ achieves a test error rate of about 14%.

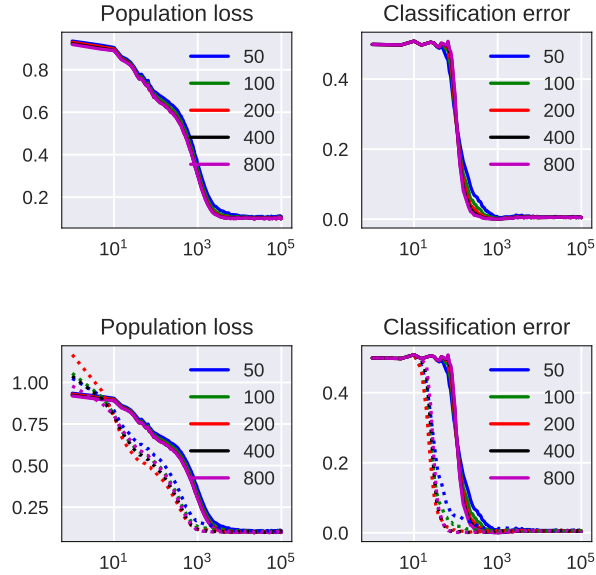


Figure 5: The performance of five 5-layers fully-connected networks on isotropic Gaussians classification, plotted against training iteration. Here for each network, $n = 50, 100, 200, 400, 800$ respectively, σ is the ReLU, and the learning rate $\alpha = 0.001$. Top row: we initialize with $\tau_1 = \sqrt{2}$, $\mu_2 = 1$, $\tau_2 = 0.1$, $\mu_3 = 0$ and $\tau_3 = 0$. Bottom row: aside from the same initialization (solid lines), we perform another initialization that differs by $\tau_2 = 3$ (dotted lines).

Acknowledgement

The work was partially supported by NSF through grants CCF-1714305 and IIS-1741162, and the William R. Hewlett Stanford Graduate Fellowship. The author would like to thank Andrea Montanari and Huy Tuan Pham for many helpful and inspiring discussions and their encouragement.

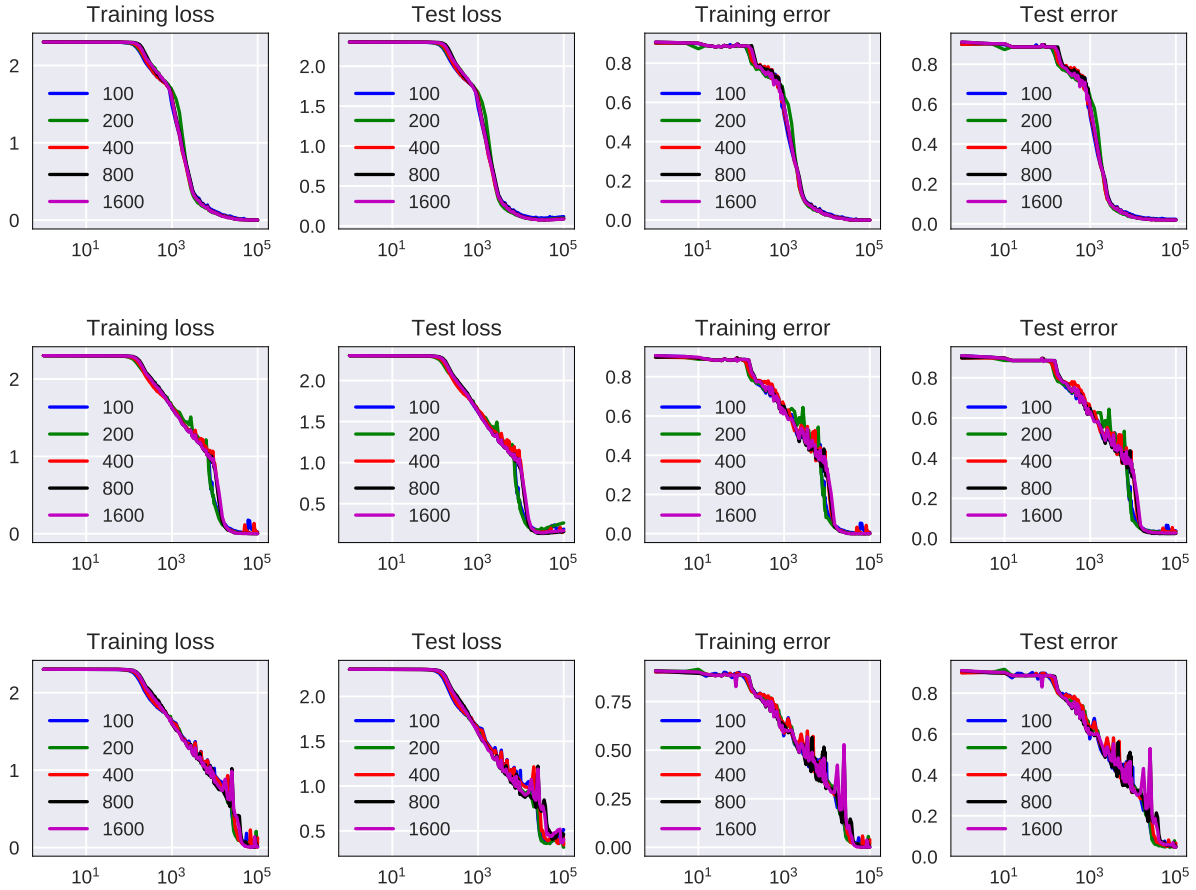


Figure 6: The performance of five fully-connected networks on MNIST classification, plotted against training iteration, in each plot. Here for each network, $n = 100, 200, 400, 800, 1600$ respectively, σ is the ReLU, and the learning rate $\alpha = 0.01$. We initialize with $\tau_1 = \sqrt{2}$, $\mu_2 = 1$, $\tau_2 = 0.1$, $\mu_3 = 0$ and $\tau_3 = 0$. From the top row: 3-layers networks, 4-layers networks and 5-layers networks.

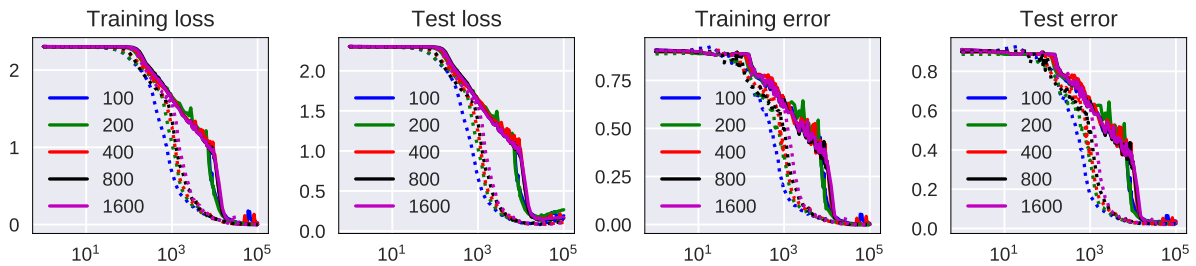


Figure 7: The performance of 4-layers fully-connected networks on MNIST classification, plotted against training iteration, in each plot. For each network, $n = 100, 200, 400, 800, 1600$ respectively, σ is the ReLU, and the learning rate $\alpha = 0.01$. We initialize with $\tau_1 = \sqrt{2}$, $\mu_2 = 1$, $\mu_3 = 0$, $\tau_3 = 0$, with $\tau_2 = 0.1$ for the solid lines and $\tau_2 = 2$ for the dotted lines.

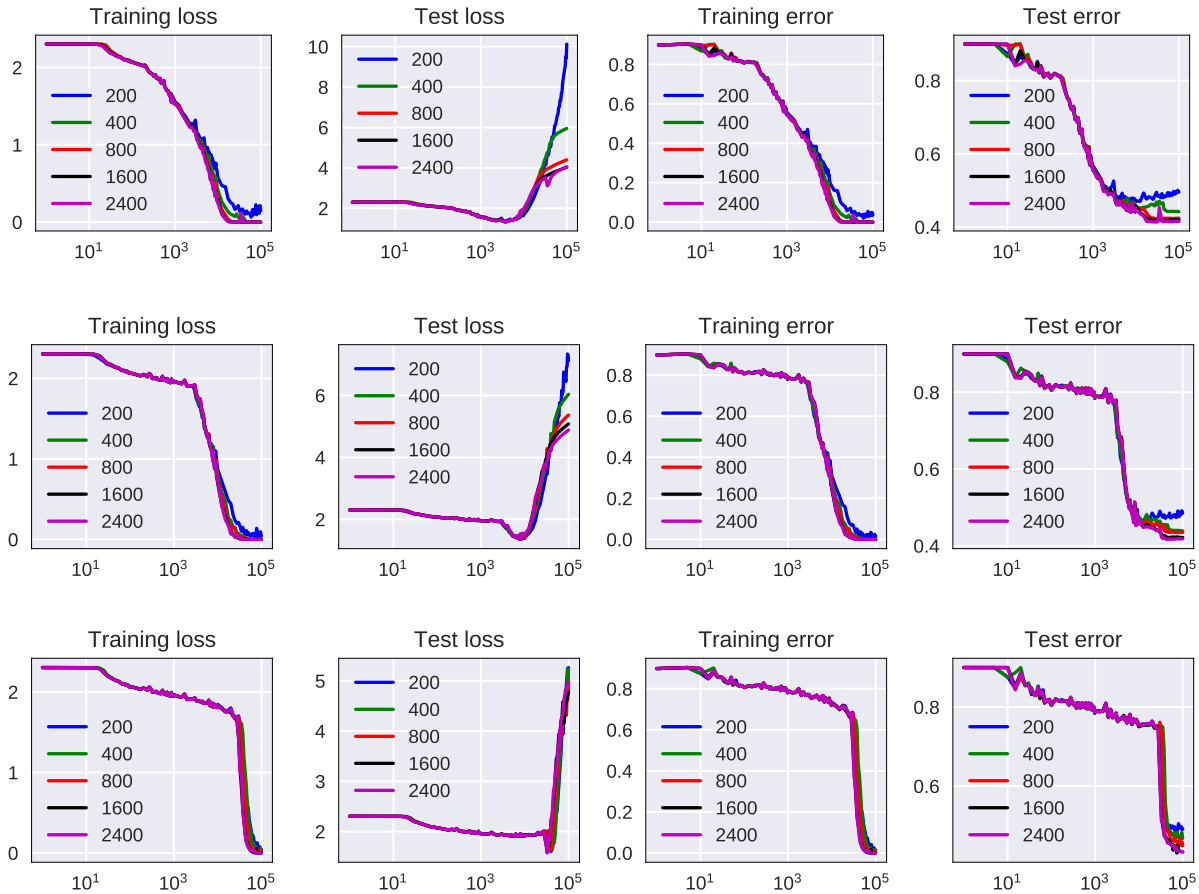


Figure 8: The performance of five fully-connected networks on CIFAR-10 classification, plotted against training iteration, in each plot. For each network, $n = 200, 400, 800, 1600, 2400$ respectively, σ is the ReLU, and the learning rate $\alpha = 0.07$. We initialize with $\tau_1 = \sqrt{2}$, $\mu_2 = 1$, $\tau_2 = 0.1$, $\mu_3 = 0$ and $\tau_3 = 0$. From the top row: 3-layers networks, 4-layers networks and 5-layers networks.

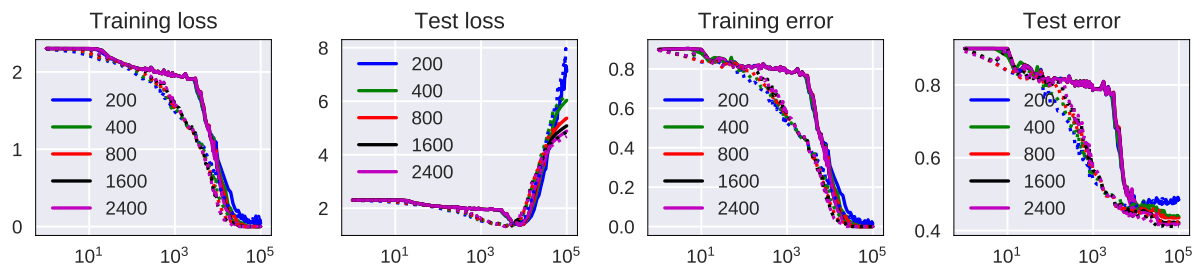


Figure 9: The performance of 4-layers fully-connected networks on CIFAR-10 classification, plotted against training iteration, in each plot. For each network, $n = 200, 400, 800, 1600, 2400$ respectively, σ is the ReLU, and the learning rate $\alpha = 0.07$. We initialize with $\tau_1 = \sqrt{2}$, $\mu_2 = 1$, $\mu_3 = 0$, $\tau_3 = 0$, with $\tau_2 = 0.1$ for the solid lines and $\tau_2 = 2$ for the dotted lines.

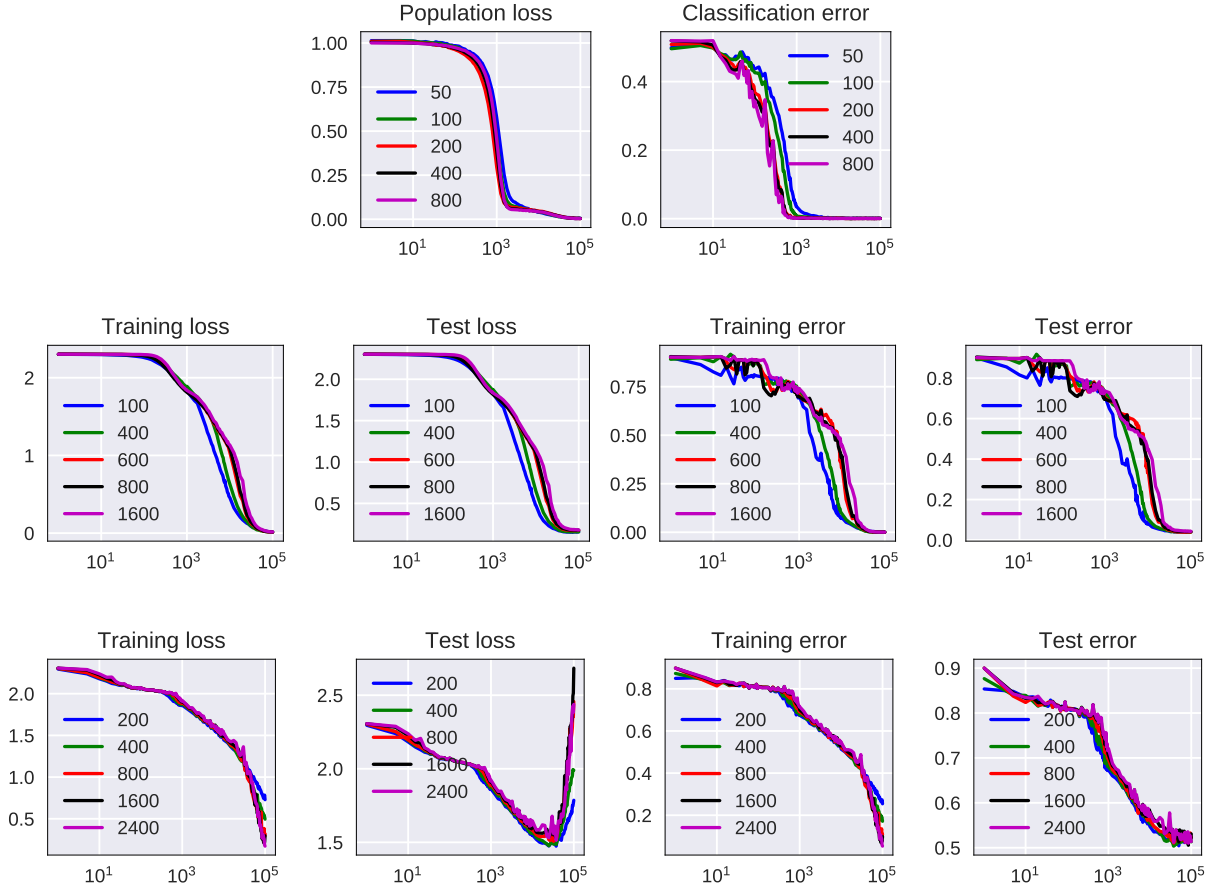


Figure 10: The performance of several fully-connected networks, plotted against training iteration, in each plot. Here the activation $\sigma = \tanh$. We choose $\tau_1 = \sqrt{2}$, $\mu_2 = 1$, $\mu_3 = 0$ and $\tau_3 = 0$ in all plots. First row: isotropic Gaussians task, 5 layers, $n = 50, 100, 200, 400, 800$, $\tau_2 = 3$, and annealed learning rate $\alpha_k = 0.003k^{-0.1}$ for $k \geq 1$ the SGD iteration. Second row: MNIST task, 4 layers, $n = 100, 400, 600, 800, 1600$, $\tau_2 = 2$, and $\alpha_k = 0.01k^{-0.1}$. Third row: CIFAR-10 task, 4 layers, $n = 200, 400, 800, 1600, 2400$, $\tau_2 = 2$, and $\alpha_k = 0.2k^{-0.1}$.

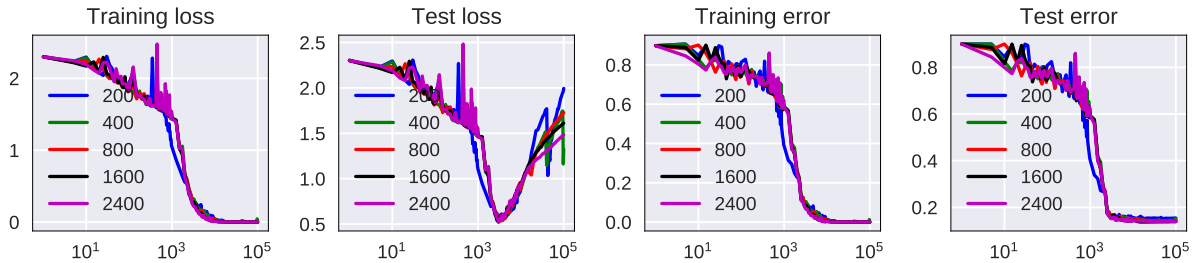


Figure 11: The performance of five 4-layers fully-connected networks on CIFAR-10 classification with VGG16 features, plotted against training iteration, in each plot. Here $n = 200, 400, 800, 1600, 2400$, σ is the ReLU, $\alpha = 0.02$, $\tau_1 = \sqrt{2}$, $\mu_2 = 1$, $\tau_2 = 0.1$, $\mu_3 = 0$, $\tau_3 = 0$.

A A heuristic derivation for the mean field limit of multilayer networks

We first recall the setting, as well as the formalism, in Section 3. We also recall the two properties, as discussed in Section 2.3: marginal uniformity and self-averaging. These properties still hold in the multilayer case, since symmetry among the neurons of the same layer holds. To make use of these properties, we represent each neuron with the following (see also Fig. 4):

- At the first layer, neuron i is represented by $(\boldsymbol{\theta}_{1,i}, \mathbf{w}_{1,i}) \in \mathbb{R}^q \times \mathcal{F}_1$, where $\mathbf{w}_{1,i}$ is the i -th row of \mathbf{W}_1 and $\boldsymbol{\theta}_{1,i}$ is the i -th element of $\boldsymbol{\Theta}_1$.
- At layer $\ell \geq 2$, neuron j is represented by $(\boldsymbol{\theta}_{\ell,j}, \nu_{\ell,j})$ where $\nu_{\ell,j} \in \mathcal{K}(\mathbb{R}^q \times \mathcal{F}_\ell, \mathbb{R})$ is a stochastic kernel and $\boldsymbol{\theta}_{\ell,j}$ is the j -th element of $\boldsymbol{\Theta}_\ell$. Neuron j generates the weight $w_{\ell,ji}$ (the (j, i) -th entry of \mathbf{W}_ℓ) according to $\nu_{2,j}(\cdot | \boldsymbol{\theta}_{1,i}, \mathbf{w}_{1,i})$ if $\ell = 2$ and $\nu_{\ell,j}(\cdot | \boldsymbol{\theta}_{\ell-1,i}, \text{CE}\{\nu_{\ell-1,i}\})$ otherwise.

We are now ready to give a heuristic derivation of the connection between the three-layers network and the formal system.

Forward pass.

Let us derive Eq. (39) from Eq. (38). We have for large n_1 , at each neuron j of the second layer for $j \in [n_2]$:

$$h_{2,j} = \frac{1}{n_1} \langle \mathbf{w}_{2,j}, \sigma_1(\boldsymbol{\Theta}_1, \mathbf{W}_1 \mathbf{x}) \rangle \approx \int w \sigma_1(\boldsymbol{\theta}, H_1(\mathbf{w}; \mathbf{x})) \nu_{2,j}(dw | \boldsymbol{\theta}, \mathbf{w}) \rho_1(d\boldsymbol{\theta}, d\mathbf{w}),$$

which replaces the empirical measure $\text{Emp}\left(\{\boldsymbol{\theta}_{1,i}, \mathbf{w}_{1,i}, w_{2,ji}\}_{i \in [n_1]}\right)$ with $\nu_{2,j} \rho_1$, by the self-averaging property. Here we note that $h_{2,j}$'s for different neuron j 's involve the same $\boldsymbol{\Theta}_1$ and \mathbf{W}_1 of the first layer. This is reflected by the use of ρ_1 independent of j . By setting

$$f_{2,j}(\boldsymbol{\theta}, \mathbf{w}) = \text{CE}\{\nu_{2,j}\}(\boldsymbol{\theta}, \mathbf{w}) = \int w \nu_{2,j}(dw | \boldsymbol{\theta}, \mathbf{w}),$$

we obtain

$$h_{2,j} \approx H_2(f_{2,j}; \mathbf{x}, \rho_1).$$

Consequently,

$$h_{3,j} = \frac{1}{n_2} \langle \mathbf{w}_{3,j}, \sigma_2(\boldsymbol{\Theta}_2, \mathbf{h}_2) \rangle \approx \frac{1}{n_2} \sum_{i=1}^{n_2} w_{3,ji} \sigma_2(\boldsymbol{\theta}_{2,i}, H_2(f_{2,i}; \mathbf{x}, \rho_1)).$$

The same argument then gives us:

$$h_{3,j} \approx \int w \sigma_2(\boldsymbol{\theta}, H_2(f; \mathbf{x}, \rho_1)) \nu_{3,j}(dw | \boldsymbol{\theta}, f) \rho_2(d\boldsymbol{\theta}, df) = H_3(f_{3,j}; \mathbf{x}, \rho_1, \rho_2),$$

in which we set $f_{3,j} = \text{CE}\{\nu_{3,j}\}$. Similarly, performing a chain of the same argument, we thus get, for $\ell = 2, \dots, L$:

$$h_{\ell,j} \approx H_\ell(f_{\ell,j}; \mathbf{x}, \{\rho_i\}_{i=1}^{\ell-1}), \quad f_{\ell,j} = \text{CE}\{\nu_{\ell,j}\}. \quad (40)$$

This yields

$$\hat{y}_n(\mathbf{x}; \mathcal{W}) = \frac{1}{n_L} \sum_{i=1}^{n_L} \sigma_L(\boldsymbol{\theta}_{L,i}, h_{L,i}) \approx \int \sigma_L(\boldsymbol{\theta}, H_L(f; \mathbf{x}, \{\rho_i\}_{i=1}^{L-1})) \rho_L(d\boldsymbol{\theta}, df) = \hat{y}(\mathbf{x}; \boldsymbol{\rho}).$$

Note that ρ_1 is a surrogate measure of $\text{Emp}(\{\boldsymbol{\theta}_{1,i}, \mathbf{w}_{1,i}\}_{i \in [n_1]})$, and for $\ell = 2, \dots, L$, ρ_ℓ is that of $\text{Emp}(\{\boldsymbol{\theta}_{\ell,i}, \text{CE}\{\nu_{\ell,i}\}\}_{i \in [n_\ell]})$.

Backward pass.

We have from Eq. (40):

$$\begin{aligned} \left(\tilde{\nabla}_{\boldsymbol{\theta}_L} \hat{y}_n(\mathbf{x}; \mathcal{W})\right)_j &\approx \nabla_1 \sigma_L(\boldsymbol{\theta}_{L,j}, H_L(f_{L,j}; \mathbf{x}, \{\rho_i\}_{i=1}^{L-1})) = \Delta_{\boldsymbol{\theta},L}(\boldsymbol{\theta}_{L,j}, f_{L,j}; \mathbf{x}, \{\rho_i\}_{i=1}^{L-1}), \\ \left(\tilde{\nabla}_{h_L} \hat{y}_n(\mathbf{x}; \mathcal{W})\right)_j &\approx \partial_2 \sigma_L(\boldsymbol{\theta}_{L,j}, H_L(f_{L,j}; \mathbf{x}, \{\rho_i\}_{i=1}^{L-1})) = \Delta_{H,L}(\boldsymbol{\theta}_{L,j}, f_{L,j}; \mathbf{x}, \{\rho_i\}_{i=1}^{L-1}). \end{aligned} \quad (41)$$

Consider $\tilde{\nabla}_{\boldsymbol{\theta}_{L-1}} \hat{y}_n(\mathbf{x}; \mathcal{W})$:

$$\begin{aligned} \left(\tilde{\nabla}_{\boldsymbol{\theta}_{L-1}} \hat{y}_n(\mathbf{x}; \mathcal{W})\right)_j &= \left(\frac{1}{n_L} \sum_{k=1}^{n_L} w_{L,kj} \left(\tilde{\nabla}_{h_L} \hat{y}_n(\mathbf{x}; \mathcal{W})\right)_k\right) \nabla_1 \sigma_{L-1}(\boldsymbol{\theta}_{L-1,j}, h_{L-1,j}) \\ &\approx \left(\frac{1}{n_L} \sum_{k=1}^{n_L} w_{L,kj} \Delta_{H,L}(\boldsymbol{\theta}_{L,k}, f_{L,k}; \mathbf{x}, \{\rho_i\}_{i=1}^{L-1})\right) \\ &\quad \times \nabla_1 \sigma_{L-1}(\boldsymbol{\theta}_{L-1,j}, H_{L-1}(f_{L-1,j}; \mathbf{x}, \{\rho_i\}_{i=1}^{L-2})). \end{aligned}$$

Recall that $w_{L,kj} \sim \nu_{L,k}(\cdot | \boldsymbol{\theta}_{L-1,j}, f_{L-1,j})$, $f_{L,k} = \text{CE}\{\nu_{L,k}\}$, and that neuron k of layer L is represented by $(\boldsymbol{\theta}_{L,k}, \nu_{L,k})$. By the self-averaging property:

$$\begin{aligned} \left(\tilde{\nabla}_{\boldsymbol{\theta}_{L-1}} \hat{y}_n(\mathbf{x}; \mathcal{W})\right)_j &\approx \left(\int f(\boldsymbol{\theta}_{L-1,j}, f_{L-1,j}) \Delta_{H,L}(\boldsymbol{\theta}, f; \mathbf{x}, \{\rho_i\}_{i=1}^{L-1}) \rho_L(d\boldsymbol{\theta}, df)\right) \\ &\quad \times \nabla_1 \sigma_{L-1}(\boldsymbol{\theta}_{L-1,j}, H_{L-1}(f_{L-1,j}; \mathbf{x}, \{\rho_i\}_{i=1}^{L-2})) \\ &= \Delta_{\boldsymbol{\theta},L-1}(\boldsymbol{\theta}_{L-1,j}, f_{L-1,j}; \mathbf{x}, \boldsymbol{\rho}), \end{aligned}$$

and similarly,

$$\left(\tilde{\nabla}_{h_{L-1}} \hat{y}_n(\mathbf{x}; \mathcal{W})\right)_j \approx \Delta_{H,L-1}(\boldsymbol{\theta}_{L-1,j}, f_{L-1,j}; \mathbf{x}, \boldsymbol{\rho}).$$

Performing the same argument and recalling that $f_{\ell,j} = \text{CE}\{\nu_{\ell,j}\}$, we obtain that

$$\left(\tilde{\nabla}_{\boldsymbol{\theta}_\ell} \hat{y}_n(\mathbf{x}; \mathcal{W})\right)_j \approx \Delta_{\boldsymbol{\theta},\ell}(\boldsymbol{\theta}_{\ell,j}, f_{\ell,j}; \mathbf{x}, \boldsymbol{\rho}), \quad \ell = 2, \dots, L-1, \quad (42)$$

$$\left(\tilde{\nabla}_{h_\ell} \hat{y}_n(\mathbf{x}; \mathcal{W})\right)_j \approx \Delta_{H,\ell}(\boldsymbol{\theta}_{\ell,j}, f_{\ell,j}; \mathbf{x}, \boldsymbol{\rho}), \quad \ell = 2, \dots, L-1,$$

$$\left(\tilde{\nabla}_{\boldsymbol{\theta}_1} \hat{y}_n(\mathbf{x}; \mathcal{W})\right)_j \approx \Delta_{\boldsymbol{\theta},1}(\boldsymbol{\theta}_{1,j}, \mathbf{w}_{1,j}; \mathbf{x}, \boldsymbol{\rho}), \quad (43)$$

$$\left(\tilde{\nabla}_{h_1} \hat{y}_n(\mathbf{x}; \mathcal{W})\right)_j \approx \Delta_{H,1}(\boldsymbol{\theta}_{1,j}, \mathbf{w}_{1,j}; \mathbf{x}, \boldsymbol{\rho}).$$

Finally, it is then easy to see that

$$\left(\tilde{\nabla}_{\mathbf{W}_L} \hat{y}_n(\mathbf{x}; \mathcal{W})\right)_{ij} \approx \Delta_{W,L}(\boldsymbol{\theta}_{L,i}, f_{L,i}, \boldsymbol{\theta}_{L-1,i}, f_{L-1,i}; \mathbf{x}, \{\rho_i\}_{i=1}^{L-1}), \quad (44)$$

$$\left(\tilde{\nabla}_{\mathbf{W}_\ell} \hat{y}_n(\mathbf{x}; \mathcal{W})\right)_{ij} \approx \Delta_{W,\ell}(\boldsymbol{\theta}_{\ell,i}, f_{\ell,i}, \boldsymbol{\theta}_{\ell-1,j}, f_{\ell-1,j}; \mathbf{x}, \boldsymbol{\rho}), \quad \ell = 3, \dots, L-1, \quad (45)$$

$$\left(\tilde{\nabla}_{\mathbf{W}_2} \hat{y}_n(\mathbf{x}; \mathcal{W})\right)_{ij} \approx \Delta_{W,2}(\boldsymbol{\theta}_{2,i}, f_{2,i}, \boldsymbol{\theta}_{1,j}, \mathbf{w}_{1,j}; \mathbf{x}, \boldsymbol{\rho}), \quad (46)$$

$$\left(\tilde{\nabla}_{\mathbf{W}_1} \hat{y}_n(\mathbf{x}; \mathcal{W})\right)_i \approx \Delta_{W,1}(\boldsymbol{\theta}_{1,i}, \mathbf{w}_{1,i}; \mathbf{x}, \boldsymbol{\rho}), \quad (47)$$

where $\left(\tilde{\nabla}_{\mathbf{W}_1} \hat{y}_n(\mathbf{x}; \mathcal{W})\right)_i$ is the i -th row of $\tilde{\nabla}_{\mathbf{W}_1} \hat{y}_n(\mathbf{x}; \mathcal{W})$.

Learning dynamics.

We now connect the evolution dynamics of the formal system with the SGD dynamics of the neural network. Similar to the three-layers case in Section 2.3, we first take $t = k\alpha$ and $\alpha \downarrow 0$ to obtain time continuum and in-expectation property w.r.t. \mathcal{P} from the SGD dynamics:

$$\begin{aligned} \frac{d}{dt} \mathbf{W}_\ell^t &= -\mathbb{E}_{\mathcal{P}} \left\{ \partial_2 \mathcal{L}(y, \hat{y}_n(\mathbf{x}; \mathcal{W}^t)) \tilde{\nabla}_{\mathbf{W}_\ell} \hat{y}_n(\mathbf{x}; \mathcal{W}^t) \right\}, \\ \frac{d}{dt} \boldsymbol{\Theta}_\ell^t &= -\mathbb{E}_{\mathcal{P}} \left\{ \partial_2 \mathcal{L}(y, \hat{y}_n(\mathbf{x}; \mathcal{W}^t)) \tilde{\nabla}_{\boldsymbol{\Theta}_\ell} \hat{y}_n(\mathbf{x}; \mathcal{W}^t) \right\}, \quad \ell = 1, \dots, L, \end{aligned}$$

where $\mathcal{W}^t = \{\mathbf{W}_1^t, \dots, \mathbf{W}_L^t, \boldsymbol{\Theta}_1^t, \dots, \boldsymbol{\Theta}_L^t\}$. Given this, at any time t , we represent neuron i of the first layer and neuron j of layer $\ell \geq 2$ with respectively $(\boldsymbol{\theta}_{1,i}^t, \mathbf{w}_{1,i}^t)$ and $(\boldsymbol{\theta}_{\ell,j}^t, \nu_{\ell,j}^t)$, whose meanings accord with the representation described at the beginning of Appendix A. We also define $f_{\ell,j}^t = \text{CE}\{\nu_{\ell,j}^t\}$ for $j \in [n_\ell]$ and $\ell = 2, \dots, L$. We let $\tilde{\rho}_1^t$ be the surrogate measure of $\text{Emp}\left(\left\{\boldsymbol{\theta}_{1,i}^t, \mathbf{w}_{1,i}^t\right\}_{i \in [n_1]}\right)$ and $\tilde{\rho}_\ell^t$ be that of $\text{Emp}\left(\left\{\boldsymbol{\theta}_{\ell,i}^t, \text{CE}\{\nu_{\ell,i}^t\}\right\}_{i \in [n_\ell]}\right)$ for $\ell = 2, \dots, L$. Let $\tilde{\boldsymbol{\rho}}^t = \{\tilde{\rho}_\ell^t\}_{\ell=1}^L$.

It is easy to see from Eq. (41)-(47) that

$$\frac{d}{dt} \mathbf{w}_{1,j}^t \approx G_{W,1}(\boldsymbol{\theta}_{1,j}^t, \mathbf{w}_{1,j}^t; \tilde{\boldsymbol{\rho}}^t), \quad (48)$$

$$\frac{d}{dt} w_{2,ij}^t \approx G_{f,2}(\boldsymbol{\theta}_{2,i}^t, f_{2,i}^t, \boldsymbol{\theta}_{1,j}^t, \mathbf{w}_{1,j}^t; \tilde{\boldsymbol{\rho}}^t), \quad (49)$$

$$\frac{d}{dt} w_{\ell,ij}^t \approx G_{f,\ell}(\boldsymbol{\theta}_{\ell,i}^t, f_{\ell,i}^t, \boldsymbol{\theta}_{\ell-1,j}^t, f_{\ell-1,j}^t; \tilde{\boldsymbol{\rho}}^t), \quad \ell = 3, \dots, L, \quad (50)$$

$$\frac{d}{dt} \boldsymbol{\theta}_{1,j}^t \approx G_{\theta,1}(\boldsymbol{\theta}_{1,j}^t, \mathbf{w}_{1,j}^t; \tilde{\boldsymbol{\rho}}^t), \quad (51)$$

$$\frac{d}{dt} \boldsymbol{\theta}_{\ell,j}^t \approx G_{\theta,\ell}(\boldsymbol{\theta}_{\ell,j}^t, f_{\ell,j}^t; \tilde{\boldsymbol{\rho}}^t), \quad \ell = 2, \dots, L. \quad (52)$$

Applying the marginal uniformity property to Eq. (48) and Eq. (51), we have $\text{Law}(\boldsymbol{\theta}_{1,j}^t, \mathbf{w}_{1,j}^t)$ is independent of j , and thanks to the self-averaging property in addition, we obtain $\text{Law}(\boldsymbol{\theta}_{1,j}^t, \mathbf{w}_{1,j}^t) \approx \tilde{\rho}_1^t$.

Observe that in Eq. (49), the right-hand side does not depend on $w_{2,ij}^t$, and since $w_{2,ij}^t \sim \nu_{2,i}^t \left(\cdot \mid \boldsymbol{\theta}_{1,j}^t, \mathbf{w}_{1,j}^t \right)$, we get for $\Delta t \rightarrow 0$ and any event $E \subseteq \mathbb{R}$,

$$\nu_{2,i}^{t+\Delta t} \left(E + G_{f,2} \left(\boldsymbol{\theta}_{2,i}^t, f_{2,i}^t, \boldsymbol{\theta}_{1,j}^t, \mathbf{w}_{1,j}^t; \tilde{\boldsymbol{\rho}}^t \right) \Delta t \mid \boldsymbol{\theta}_{1,j}^{t+\Delta t}, \mathbf{w}_{1,j}^{t+\Delta t} \right) \approx \nu_{2,i}^t \left(E \mid \boldsymbol{\theta}_{1,j}^t, \mathbf{w}_{1,j}^t \right).$$

This gives us

$$\begin{aligned} \frac{d}{dt} \left(f_{2,i}^t \left(\boldsymbol{\theta}_{1,j}^t, \mathbf{w}_{1,j}^t \right) \right) &= \lim_{\Delta t \rightarrow 0} \frac{1}{\Delta t} \left(\int w \nu_{2,i}^{t+\Delta t} \left(dw \mid \boldsymbol{\theta}_{1,j}^{t+\Delta t}, \mathbf{w}_{1,j}^{t+\Delta t} \right) - \int w \nu_{2,i}^t \left(dw \mid \boldsymbol{\theta}_{1,j}^t, \mathbf{w}_{1,j}^t \right) \right) \\ &\approx \lim_{\Delta t \rightarrow 0} \frac{1}{\Delta t} \left(\int \left(w + G_{f,2} \left(\boldsymbol{\theta}_{2,i}^t, f_{2,i}^t, \boldsymbol{\theta}_{1,j}^t, \mathbf{w}_{1,j}^t; \tilde{\boldsymbol{\rho}}^t \right) \Delta t \right) \nu_{2,i}^t \left(dw \mid \boldsymbol{\theta}_{1,j}^t, \mathbf{w}_{1,j}^t \right) \right. \\ &\quad \left. - \int w \nu_{2,i}^t \left(dw \mid \boldsymbol{\theta}_{1,j}^t, \mathbf{w}_{1,j}^t \right) \right) \\ &= G_{f,2} \left(\boldsymbol{\theta}_{2,i}^t, f_{2,i}^t, \boldsymbol{\theta}_{1,j}^t, \mathbf{w}_{1,j}^t; \tilde{\boldsymbol{\rho}}^t \right). \end{aligned}$$

On the other hand, from Eq. (48) and (51),

$$\begin{aligned} \frac{d}{dt} \left(f_{2,i}^t \left(\boldsymbol{\theta}_{1,j}^t, \mathbf{w}_{1,j}^t \right) \right) &= \left(\partial_t f_{2,i}^t \right) \left(\boldsymbol{\theta}_{1,j}^t, \mathbf{w}_{1,j}^t \right) + \left\langle \nabla_1 f_{2,i}^t \left(\boldsymbol{\theta}_{1,j}^t, \mathbf{w}_{1,j}^t \right), G_{\theta,1} \left(\boldsymbol{\theta}_{1,j}^t, \mathbf{w}_{1,j}^t; \tilde{\boldsymbol{\rho}}^t \right) \right\rangle \\ &\quad + \left\langle \nabla_2 f_{2,i}^t \left(\boldsymbol{\theta}_{1,j}^t, \mathbf{w}_{1,j}^t \right), G_{W,1} \left(\boldsymbol{\theta}_{1,j}^t, \mathbf{w}_{1,j}^t; \tilde{\boldsymbol{\rho}}^t \right) \right\rangle. \end{aligned}$$

We thus get:

$$\partial_t f_{2,i}^t \left(\boldsymbol{\theta}, \mathbf{w} \right) \approx \mathcal{G}_2 \left(\boldsymbol{\theta}_{2,i}^t, f_{2,i}^t, \boldsymbol{\theta}, \mathbf{w}; \tilde{\boldsymbol{\rho}}^t \right), \quad (53)$$

for $\tilde{\rho}_1^t$ -a.e. $(\boldsymbol{\theta}, \mathbf{w})$, recalling Law $\left(\boldsymbol{\theta}_{1,j}^t, \mathbf{w}_{1,j}^t \right) \approx \tilde{\rho}_1^t$ for any $j \in [n_1]$. Observe that values of $f_{2,i}^t$ at $(\boldsymbol{\theta}, \mathbf{w}) \notin \text{supp}(\tilde{\rho}_1^t)$ are used in the computation of neither the forward pass nor the backward pass at time t . As such, one can extend the dynamic (53) to all $(\boldsymbol{\theta}, \mathbf{w}) \in \mathbb{R}^q \times \mathcal{F}_1$ without affecting the prediction stated in Section 3.2. Applying the marginal uniformity and self-averaging properties again, we then obtain Law $\left(\boldsymbol{\theta}_{2,i}^t, f_{2,i}^t \right) \approx \tilde{\rho}_2^t$ for any $i \in [n_2]$. One can then perform a similar argument on Eq. (50) inductively for $\ell = 3, \dots, L$ and get:

$$\begin{aligned} \frac{d}{dt} \left(f_{\ell,i}^t \left(\boldsymbol{\theta}_{\ell-1,j}^t, f_{\ell-1,j}^t \right) \right) &\approx G_{f,\ell} \left(\boldsymbol{\theta}_{\ell,i}^t, f_{\ell,i}^t, \boldsymbol{\theta}_{\ell-1,j}^t, f_{\ell-1,j}^t; \tilde{\boldsymbol{\rho}}^t \right), \\ \frac{d}{dt} \left(f_{\ell,i}^t \left(\boldsymbol{\theta}_{\ell-1,j}^t, f_{\ell-1,j}^t \right) \right) &= \left(\partial_t f_{\ell,i}^t \right) \left(\boldsymbol{\theta}_{\ell-1,j}^t, f_{\ell-1,j}^t \right) + \left\langle \nabla_1 f_{\ell,i}^t \left(\boldsymbol{\theta}_{\ell-1,j}^t, f_{\ell-1,j}^t \right), G_{\theta,\ell} \left(\boldsymbol{\theta}_{\ell-1,j}^t, f_{\ell-1,j}^t; \tilde{\boldsymbol{\rho}}^t \right) \right\rangle \\ &\quad + \mathcal{D}_2 f_{\ell,i}^t \left\{ \boldsymbol{\theta}_{\ell-1,j}^t, f_{\ell-1,j}^t \right\} \left(\partial_t f_{\ell-1,j}^t \right), \end{aligned}$$

which yields

$$\partial_t f_{\ell,i}^t \left(\boldsymbol{\theta}, f \right) \approx \mathcal{G}_\ell \left(\boldsymbol{\theta}_{\ell,i}^t, f_{\ell,i}^t, \boldsymbol{\theta}, f; \tilde{\boldsymbol{\rho}}^t \right) \quad \forall (\boldsymbol{\theta}, f) \in \mathbb{R}^q \times \mathcal{F}_{\ell-1}, \quad \text{Law} \left(\boldsymbol{\theta}_{\ell,i}^t, f_{\ell,i}^t \right) \approx \tilde{\rho}_\ell^t,$$

for all $i \in [n_\ell]$. Hence, if $\tilde{\rho}_\ell^0 = \rho_\ell^0$ for all $\ell \in [L]$, then $\tilde{\rho}_\ell^t \approx \rho_\ell^t$ for all $\ell \in [L]$ at any time t . This completes the derivation.

Finally we note that the initialization in the prediction statement in Section 3.2 is sufficient to ensure firstly that symmetry among the neurons is attained at initialization and hence at all subsequent time, and secondly $\tilde{\rho}_\ell^0 = \rho_\ell^0$ for all $\ell \in [L]$.

B Statics: equivalence of the optima for multilayer networks

We recall the multilayer network (38) and its formal system (39). Also recall that $n_\ell = n_\ell(n) \rightarrow \infty$ as $n \rightarrow \infty$. In the following, we argue that

$$\lim_{n \rightarrow \infty} \inf_{\mathcal{W}} \mathbb{E}_{\mathcal{P}} \{ \mathcal{L}(y, \hat{y}_n(\mathbf{x}; \mathcal{W})) \} = \inf_{\underline{\rho}} \mathbb{E}_{\mathcal{P}} \{ \mathcal{L}(y, \hat{y}(\mathbf{x}; \underline{\rho})) \},$$

under certain assumptions to be stated below. This result is similar to, though not as quantitative as, Eq. (4) of the two-layers case. To show the above, it is decomposed into the two inequalities:

$$\inf_{\underline{\rho}} \mathbb{E}_{\mathcal{P}} \{ \mathcal{L}(y, \hat{y}(\mathbf{x}; \underline{\rho})) \} \leq \inf_{\mathcal{W}} \mathbb{E}_{\mathcal{P}} \{ \mathcal{L}(y, \hat{y}_n(\mathbf{x}; \mathcal{W})) \}, \quad (54)$$

$$\limsup_{n \rightarrow \infty} \inf_{\mathcal{W}} \mathbb{E}_{\mathcal{P}} \{ \mathcal{L}(y, \hat{y}_n(\mathbf{x}; \mathcal{W})) \} \leq \inf_{\underline{\rho}} \mathbb{E}_{\mathcal{P}} \{ \mathcal{L}(y, \hat{y}(\mathbf{x}; \underline{\rho})) \}. \quad (55)$$

Then the thesis follows immediately.

Below we shall let C denote any (immaterial) constant, and similarly, $c = c(\epsilon)$ denote any “constant” that depends on ϵ – a parameter that is to be defined below. That is, C and $c(\epsilon)$ are constants that may change from line to line. We state our assumptions:

- σ_L satisfies that for some constant $C > 0$:

$$|\sigma_L(\boldsymbol{\theta}_1, h_1) - \sigma_L(\boldsymbol{\theta}_2, h_2)| \leq C(1 + \|\boldsymbol{\theta}_1\|_2 + \|\boldsymbol{\theta}_2\|_2)(\|\boldsymbol{\theta}_1 - \boldsymbol{\theta}_2\|_2 + |h_1 - h_2|), \quad (56)$$

$$|\sigma_L(\boldsymbol{\theta}, h)| \leq C(1 + \|\boldsymbol{\theta}\|_2), \quad (57)$$

for any $\boldsymbol{\theta}, \boldsymbol{\theta}_1, \boldsymbol{\theta}_2 \in \mathbb{R}^q$ and $h, h_1, h_2 \in \mathbb{R}$.

- For each $\ell = 1, \dots, L-1$, σ_ℓ satisfies that for some constant $C > 0$:

$$|\sigma_\ell(\boldsymbol{\theta}_1, h_1) - \sigma_\ell(\boldsymbol{\theta}_2, h_2)| \leq C(\|\boldsymbol{\theta}_1 - \boldsymbol{\theta}_2\|_2 + |h_1 - h_2|), \quad (58)$$

$$\|\sigma_\ell\|_\infty \leq C, \quad (59)$$

for any $\boldsymbol{\theta}_1, \boldsymbol{\theta}_2 \in \mathbb{R}^q$ and $h_1, h_2 \in \mathbb{R}$.

- \mathcal{L} satisfies that for some constant $C > 0$:

$$|\mathcal{L}(y_1, y_2) - \mathcal{L}(y_3, y_4)| \leq C(1 + |y_1| + |y_2| + |y_3| + |y_4|)(|y_1 - y_3| + |y_2 - y_4|), \quad (60)$$

for any $y_1, y_2, y_3, y_4 \in \mathbb{R}$.

- There exists a constant C such that the data satisfies:

$$\mathcal{P}(|y| > C) = 0. \quad (61)$$

- For all $\epsilon > 0$ sufficiently small, there exists $\underline{\rho} = \{\rho_\ell\}_{\ell=1}^L$ such that

$$\mathbb{E}_{\mathcal{P}} \{ \mathcal{L}(y, \hat{y}(\mathbf{x}; \underline{\rho})) \} \leq \inf_{\underline{\rho}'} \mathbb{E}_{\mathcal{P}} \{ \mathcal{L}(y, \hat{y}(\mathbf{x}; \underline{\rho}')) \} + \epsilon, \quad (62)$$

as well as that

$$\rho_L(\{\|\boldsymbol{\theta}\|_2 > c\}) = 0, \quad \rho_\ell(\{f \in \mathcal{F}_\ell: \|f\|_\infty > c\}) = 0, \quad \ell = 2, \dots, L, \quad (63)$$

for some $c = c(\epsilon)$.

B.1 Derivation of Eq. (54)

For $\epsilon > 0$, we take $\mathcal{W} = \{\mathbf{W}_1, \dots, \mathbf{W}_L, \Theta_1, \dots, \Theta_L\}$ that yields

$$\mathbb{E}_{\mathcal{P}} \{\mathcal{L}(y, \hat{y}_n(\mathbf{x}; \mathcal{W}))\} \leq \inf_{\mathcal{W}'} \mathbb{E}_{\mathcal{P}} \{\mathcal{L}(y, \hat{y}_n(\mathbf{x}; \mathcal{W}'))\} + \epsilon.$$

Let $\Theta_\ell = (\theta_{\ell,i})_{i \in [n_\ell]}$, $\mathbf{W}_1 = (\mathbf{w}_{1,i})_{i \in [n_1]}$ and $\mathbf{W}_\ell = (w_{\ell,ij})_{i \in [n_\ell], j \in [n_{\ell-1}]}$. We construct $\underline{\rho} = \{\rho_\ell\}_{\ell=1}^L$ as follows. Take

$$\rho_1 = \frac{1}{n_1} \sum_{i=1}^{n_1} \delta_{\theta_{1,i}, \mathbf{w}_{1,i}}.$$

We choose (any) $f_{2,i} \in \mathcal{F}_2$, for each $i \in [n_2]$, such that for any $j \in [n_1]$,

$$f_{2,i}(\theta_{1,j}, \mathbf{w}_{1,j}) = \frac{1}{|S_{1,j}|} \sum_{k \in S_{1,j}} w_{2,ik}, \quad S_{1,j} = \{k \in [n_1] : (\theta_{1,k}, \mathbf{w}_{1,k}) = (\theta_{1,j}, \mathbf{w}_{1,j})\}.$$

We then take

$$\rho_2 = \frac{1}{n_2} \sum_{i=1}^{n_2} \delta_{\theta_{2,i}, f_{2,i}}.$$

We continue this process inductively, i.e. for $\ell \geq 3$, we choose $f_{\ell,i} \in \mathcal{F}_\ell$, for each $i \in [n_\ell]$, such that for any $j \in [n_{\ell-1}]$,

$$f_{\ell,i}(\theta_{\ell-1,j}, f_{\ell-1,j}) = \frac{1}{|S_{\ell-1,j}|} \sum_{k \in S_{\ell-1,j}} w_{\ell,ik}, \quad S_{\ell-1,j} = \{k \in [n_{\ell-1}] : (\theta_{\ell-1,k}, f_{\ell-1,k}) = (\theta_{\ell-1,j}, f_{\ell-1,j})\},$$

and we take

$$\rho_\ell = \frac{1}{n_\ell} \sum_{i=1}^{n_\ell} \delta_{\theta_{\ell,i}, f_{\ell,i}}.$$

Then it is easy to check that

$$\mathbb{E}_{\mathcal{P}} \{\mathcal{L}(y, \hat{y}_n(\mathbf{x}; \mathcal{W}))\} = \mathbb{E}_{\mathcal{P}} \{\mathcal{L}(y, \hat{y}(\mathbf{x}; \underline{\rho}))\}.$$

This yields Eq. (54), since ϵ is arbitrary.

B.2 Derivation of Eq. (55)

For $\epsilon > 0$ sufficiently small, we take $\underline{\rho} = \{\rho_\ell\}_{\ell=1}^L$ that satisfies Assumptions (62) and (63). Let us generate $\mathcal{W} = \{\mathbf{W}_1, \dots, \mathbf{W}_L, \Theta_1, \dots, \Theta_L\}$ at random as follows. First we generate $\{(\theta_{1,i}, \mathbf{w}_{1,i})\}_{i \in [n_1]} \sim \rho_1$ i.i.d. and form $\mathbf{W}_1 = (\mathbf{w}_{1,i})_{i \in [n_1]}$ and $\Theta_1 = (\theta_{1,i})_{i \in [n_1]}$. Then inductively for $\ell = 2, \dots, L$, we generate $\{(\theta_{\ell,i}, f_{\ell,i})\}_{i \in [n_\ell]} \sim \rho_\ell$ i.i.d., all independently of each other and of $\{(\theta_{1,i}, \mathbf{w}_{1,i})\}_{i \in [n_1]}$, and form $\mathbf{W}_2 = (f_{2,i}(\theta_{1,j}, \mathbf{w}_{1,j}))_{i \in [n_2], j \in [n_1]}$, $\mathbf{W}_\ell = (f_{\ell,i}(\theta_{\ell-1,j}, f_{\ell-1,j}))_{i \in [n_\ell], j \in [n_{\ell-1}]}$ and $\Theta_\ell = (\theta_{\ell,i})_{i \in [n_\ell]}$. We shall argue that

$$\mathbb{E}_{\mathcal{W}} \{\mathbb{E}_{\mathcal{P}} \{\mathcal{L}(y, \hat{y}_n(\mathbf{x}; \mathcal{W}))\}\} \leq \mathbb{E}_{\mathcal{P}} \{\mathcal{L}(y, \hat{y}(\mathbf{x}; \underline{\rho}))\} + c(\epsilon) \sum_{\ell=1}^L \frac{1}{\sqrt{n_\ell}}. \quad (64)$$

This implies

$$\inf_{\mathcal{W}} \mathbb{E}_{\mathcal{P}} \{ \mathcal{L}(y, \hat{y}_n(\mathbf{x}; \mathcal{W})) \} \leq \inf_{\underline{\rho}} \mathbb{E}_{\mathcal{P}} \{ \mathcal{L}(y, \hat{y}(\mathbf{x}; \underline{\rho})) \} + c(\epsilon) \sum_{\ell=1}^L \frac{1}{\sqrt{n_\ell}} + \epsilon,$$

which immediately gives Eq. (55) by taking $n \rightarrow \infty$ and then $\epsilon \rightarrow 0$. To that end, for each $\ell = 2, \dots, L$, let us define $\hat{y}_n^{(\ell)} : \mathbb{R}^{n_\ell} \mapsto \mathbb{R}$ such that

$$\hat{y}_n^{(\ell)}(\mathbf{h}_\ell) = \hat{y}_n(\mathbf{x}; \mathcal{W}).$$

Here recall that

$$\begin{aligned} \hat{y}_n(\mathbf{x}; \mathcal{W}) &= \frac{1}{n_L} \sum_{i=1}^{n_L} \sigma_L(\boldsymbol{\theta}_{L,i}, h_{L,i}), \\ \mathbf{h}_\ell &= \frac{1}{n_{\ell-1}} \mathbf{W}_\ell \sigma_{\ell-1}(\boldsymbol{\Theta}_{\ell-1}, \mathbf{h}_{\ell-1}), \quad \ell = 2, \dots, L, \\ \mathbf{h}_1 &= \mathbf{W}_1 \mathbf{x}. \end{aligned}$$

Note that in the above definition, $\hat{y}_n^{(\ell)}$ depends on $\boldsymbol{\Theta}_\ell, \dots, \boldsymbol{\Theta}_L, \mathbf{W}_{\ell+1}, \dots, \mathbf{W}_L$ and \mathbf{x} , which are not displayed to lighten the notation. In the following, the dependency on \mathcal{W} or $\underline{\rho}$ is also not displayed. The derivation of Eq. (64) contains several steps.

Step 1. We argue that for each $\ell \geq 2$ and any $\mathbf{u}, \mathbf{v} \in \mathbb{R}^{n_\ell}$,

$$\left| \hat{y}_n^{(\ell)}(\mathbf{u}) - \hat{y}_n^{(\ell)}(\mathbf{v}) \right| \leq \frac{c(\epsilon)}{\sqrt{n_\ell}} \|\mathbf{u} - \mathbf{v}\|_2. \quad (65)$$

First, we have:

$$\begin{aligned} \left| \hat{y}_n^{(L)}(\mathbf{u}) - \hat{y}_n^{(L)}(\mathbf{v}) \right| &= \left| \frac{1}{n_L} \sum_{i=1}^{n_L} \sigma_L(\boldsymbol{\theta}_{L,i}, u_i) - \frac{1}{n_L} \sum_{i=1}^{n_L} \sigma_L(\boldsymbol{\theta}_{L,i}, v_i) \right| \\ &\stackrel{(a)}{\leq} \frac{C}{n_L} \sum_{i=1}^{n_L} (1 + \|\boldsymbol{\theta}_{L,i}\|_2) |u_i - v_i| \\ &\leq \frac{C}{n_L} \sqrt{n_L + \|\boldsymbol{\Theta}_L\|_F^2} \|\mathbf{u} - \mathbf{v}\|_2 \\ &\stackrel{(b)}{\leq} \frac{c(\epsilon)}{\sqrt{n_L}} \|\mathbf{u} - \mathbf{v}\|_2, \end{aligned}$$

where (a) is from Assumption (56), and (b) is from Assumption (63). We then show the thesis by induction. Indeed, assuming the claim for $\ell + 1$, we have:

$$\begin{aligned} \left| \hat{y}_n^{(\ell)}(\mathbf{u}) - \hat{y}_n^{(\ell)}(\mathbf{v}) \right| &= \left| \hat{y}_n^{(\ell+1)}\left(\frac{1}{n_\ell} \mathbf{W}_{\ell+1} \sigma_\ell(\boldsymbol{\Theta}_\ell, \mathbf{u})\right) - \hat{y}_n^{(\ell+1)}\left(\frac{1}{n_\ell} \mathbf{W}_{\ell+1} \sigma_\ell(\boldsymbol{\Theta}_\ell, \mathbf{v})\right) \right| \\ &\stackrel{(a)}{\leq} \frac{c(\epsilon)}{n_\ell \sqrt{n_{\ell+1}}} \|\mathbf{W}_{\ell+1} \sigma_\ell(\boldsymbol{\Theta}_\ell, \mathbf{u}) - \mathbf{W}_{\ell+1} \sigma_\ell(\boldsymbol{\Theta}_\ell, \mathbf{v})\|_2 \\ &\stackrel{(b)}{\leq} \frac{c(\epsilon)}{n_\ell \sqrt{n_{\ell+1}}} \|\mathbf{W}_{\ell+1}\|_F \|\mathbf{u} - \mathbf{v}\|_2 \\ &\stackrel{(c)}{\leq} \frac{c(\epsilon)}{\sqrt{n_\ell}} \|\mathbf{u} - \mathbf{v}\|_2, \end{aligned}$$

where (a) is by the induction hypothesis, (b) is by Assumption (58), and (c) is from Assumption (63). This shows the thesis.

Step 2. We argue that

$$\mathbb{E} \{ |\hat{y}_n(\mathbf{x}) - \hat{y}(\mathbf{x})| \} \leq c(\epsilon) \sum_{\ell=1}^L \frac{1}{\sqrt{n_\ell}}. \quad (66)$$

Notice that

$$\begin{aligned} \hat{y}_n^{(L)} \left((H_L(f_{L,i}; \mathbf{x}))_{i \in [n_L]} \right) &= \frac{1}{n_L} \sum_{i=1}^{n_L} \sigma_L(\boldsymbol{\theta}_{L,i}, H_L(f_{L,i}; \mathbf{x})), \\ \hat{y}_n^{(\ell)} \left((H_\ell(f_{\ell,i}; \mathbf{x}))_{i \in [n_\ell]} \right) &= \hat{y}_n^{(\ell+1)} \left(\frac{1}{n_\ell} \mathbf{W}_{\ell+1} \sigma_\ell \left(\boldsymbol{\Theta}_\ell, (H_\ell(f_{\ell,i}; \mathbf{x}))_{i \in [n_\ell]} \right) \right), \quad \ell = 2, \dots, L-1, \\ \hat{y}_n^{(2)} \left(\frac{1}{n_1} \mathbf{W}_2 \sigma_1 \left(\boldsymbol{\Theta}_1, \mathbf{h}_1 \right) \right) &= \hat{y}_n(\mathbf{x}). \end{aligned}$$

We thus have the following decomposition:

$$\begin{aligned} &\mathbb{E} \{ |\hat{y}_n(\mathbf{x}) - \hat{y}(\mathbf{x})| \} \\ &\leq \mathbb{E} \left\{ \left| \hat{y}(\mathbf{x}) - \frac{1}{n_L} \sum_{i=1}^{n_L} \sigma_L(\boldsymbol{\theta}_{L,i}, H_L(f_{L,i}; \mathbf{x})) \right| \right\} \\ &\quad + \sum_{\ell=2}^{L-1} \mathbb{E} \left\{ \left| \hat{y}_n^{(\ell+1)} \left((H_{\ell+1}(f_{\ell+1,i}; \mathbf{x}))_{i \in [n_{\ell+1}]} \right) - \hat{y}_n^{(\ell+1)} \left(\frac{1}{n_\ell} \mathbf{W}_{\ell+1} \sigma_\ell \left(\boldsymbol{\Theta}_\ell, (H_\ell(f_{\ell,i}; \mathbf{x}))_{i \in [n_\ell]} \right) \right) \right| \right\} \\ &\quad + \mathbb{E} \left\{ \left| \hat{y}_n^{(2)} \left((H_2(f_{2,i}; \mathbf{x}))_{i \in [n_2]} \right) - \hat{y}_n^{(2)} \left(\frac{1}{n_1} \mathbf{W}_2 \sigma_1 \left(\boldsymbol{\Theta}_1, \mathbf{h}_1 \right) \right) \right| \right\} \\ &\equiv A_L + \sum_{\ell=2}^{L-1} A_\ell + A_1. \end{aligned}$$

From Eq. (65), we have for $\ell = 2, \dots, L-1$:

$$\begin{aligned} A_\ell^2 &\leq \mathbb{E} \left\{ \left| \hat{y}_n^{(\ell+1)} \left((H_{\ell+1}(f_{\ell+1,i}; \mathbf{x}))_{i \in [n_{\ell+1}]} \right) - \hat{y}_n^{(\ell+1)} \left(\frac{1}{n_\ell} \mathbf{W}_{\ell+1} \sigma_\ell \left(\boldsymbol{\Theta}_\ell, (H_\ell(f_{\ell,i}; \mathbf{x}))_{i \in [n_\ell]} \right) \right) \right|^2 \right\} \\ &\leq \frac{c(\epsilon)}{n_{\ell+1}} \sum_{i=1}^{n_{\ell+1}} \mathbb{E} \left\{ \left(H_{\ell+1}(f_{\ell+1,i}; \mathbf{x}) - \frac{1}{n_\ell} \sum_{j=1}^{n_\ell} f_{\ell+1,i}(\boldsymbol{\theta}_{\ell,j}, f_{\ell,j}) \sigma_\ell(\boldsymbol{\theta}_{\ell,j}, H_\ell(f_{\ell,j}; \mathbf{x})) \right)^2 \right\} \\ &\stackrel{(a)}{=} \frac{c(\epsilon)}{n_\ell n_{\ell+1}} \sum_{i=1}^{n_{\ell+1}} \mathbb{E} \{ \text{Var}_\ell \{ f_{\ell+1,i}(\boldsymbol{\theta}, f) \sigma_\ell(\boldsymbol{\theta}, H_\ell(f; \mathbf{x})) \} \} \\ &\leq \frac{c(\epsilon)}{n_\ell n_{\ell+1}} \sum_{i=1}^{n_{\ell+1}} \mathbb{E} \left\{ \mathbb{E}_\ell \left\{ f_{\ell+1,i}^2(\boldsymbol{\theta}, f) \sigma_\ell^2(\boldsymbol{\theta}, H_\ell(f; \mathbf{x})) \right\} \right\} \\ &\stackrel{(b)}{\leq} \frac{c(\epsilon)}{n_\ell} \end{aligned}$$

where Var_ℓ and \mathbb{E}_ℓ indicate the variance and the mean w.r.t. $(\boldsymbol{\theta}, f) \sim \rho_\ell$. Here the factor $1/n_\ell$ in step (a) is due to $\{(\boldsymbol{\theta}_{\ell,i}, f_{\ell,i})\}_{i \in [n_\ell]} \sim \rho_\ell$ i.i.d., and step (b) is due to Assumptions (63) and (59). Similarly we have $A_1^2 \leq c(\epsilon)/n_1$ and $A_L^2 \leq c(\epsilon)/n_L$. The thesis then follows.

Step 3. From Assumptions (60) and (61), we have:

$$|\mathbb{E}_{\mathcal{W}} \{\mathbb{E}_{\mathcal{P}} \{\mathcal{L}(y, \hat{y}_n(\mathbf{x}))\}\} - \mathbb{E}_{\mathcal{P}} \{\mathcal{L}(y, \hat{y}(\mathbf{x}))\}| \leq C\mathbb{E} \{(1 + |\hat{y}_n(\mathbf{x})| + |\hat{y}(\mathbf{x})|) |\hat{y}_n(\mathbf{x}) - \hat{y}(\mathbf{x})|\}.$$

Notice that from Assumptions (57) and (63),

$$|\hat{y}_n(\mathbf{x})| \leq \frac{1}{n_L} \sum_{i=1}^{n_L} |\sigma_L(\boldsymbol{\theta}_{L,i}, h_{L,i})| \leq \frac{C}{n_L} \sum_{i=1}^{n_L} (1 + \|\boldsymbol{\theta}_{L,i}\|_2) \leq c(\epsilon).$$

Similarly, $|\hat{y}(\mathbf{x})| \leq c(\epsilon)$. Combining with Eq. (66), we arrive at Eq. (64).

C Mean field limit in multilayer convolutional neural networks

We consider convolutional neural networks (CNNs), which are most interesting when they have many layers. In a CNN, the number of neurons n_ℓ at layer ℓ is the number of filters at that layer. A simple convolutional analog of the three-layers fully-connected network (7) can be described by the following:

$$\hat{y}_n(\mathbf{x}; \mathcal{W}) = \frac{1}{n_2} \langle \boldsymbol{\beta}, \sigma_2(\mathbf{h}_2) \rangle, \quad \mathbf{h}_2 = \frac{1}{n_1} \mathbf{W}_2 \circledast \sigma_1(\mathbf{h}_1), \quad \mathbf{h}_1 = \mathbf{W}_1 \circledast \mathbf{x}.$$

Here \circledast is the operator defined by

$$\mathbf{W} \circledast \mathbf{u} = \left(\sum_{j=1}^{m_1} w_{ij} * u_j \right)_{i \in [m_2]}, \quad \mathbf{u} \in (\mathbb{R}^p)^{m_1}, \quad \mathbf{W} = (w_{ij})_{i \in [m_2], j \in [m_1]} \in (\mathbb{R}^s)^{m_2 \times m_1},$$

for a convolutional operator $*$, in which $w * u \in \mathbb{R}^{r(s,p)}$ for any $u \in \mathbb{R}^p$ and $w \in \mathbb{R}^s$, and $r(s,p)$ is an integer to be determined by the exact operation of $*$. It can be made $r(s,p) = p$ with appropriate paddings and no striding. In our context,

- $\mathbf{x} \in (\mathbb{R}^p)^d$ a p -pixels d -channels (1-dimensional) input image (e.g. $d = 3$ for an RGB image),
- $\mathbf{W}_1 \in (\mathbb{R}^{s_1})^{n_1 \times d}$ where each entry is an element in \mathbb{R}^{s_1} and the receptive field size is s_1 ,
- $\mathbf{h}_1 \in (\mathbb{R}^{r(s_1,p)})^{n_1}$, $\sigma_1 : \mathbb{R}^{r(s_1,p)} \mapsto \mathbb{R}^{p_1}$ some nonlinear mapping for $p_1 = p_1(r(s_1,p))$, and $\sigma_1(\mathbf{h}_1) \in (\mathbb{R}^{p_1})^{n_1}$ element-wise,
- $\mathbf{W}_2 \in (\mathbb{R}^{s_2})^{n_2 \times n_1}$ where each entry is an element in \mathbb{R}^{s_2} and the receptive field size is s_2 ,
- $\mathbf{h}_2 \in (\mathbb{R}^{r(s_2,p_1)})^{n_2}$, $\sigma_2 : \mathbb{R}^{r(s_2,p_1)} \mapsto \mathbb{R}^{p_2}$ some nonlinear mapping for $p_2 = p_2(r(s_2,p_1))$, and $\sigma_2(\mathbf{h}_2) \in (\mathbb{R}^{p_2})^{n_2}$ element-wise,
- $\boldsymbol{\beta} \in \mathbb{R}^{n_2 p_2}$ and $\langle \cdot, \cdot \rangle$ computes the usual Euclidean inner product after vectorizing its arguments.

The nonlinear mapping can be, as in the usual practice, a composition of a pooling operation and a scalar nonlinear activation. Now observe the similarity between this network and its fully-connected counterpart, especially the summation structure shared by both, as evident from the definition of

Layer	Structure	Output spatial dimension
1	CONV-(3, 3, n), stride (2, 2) — ReLU	16×16
2	CONV-(3, 3, n), stride (2, 2) — ReLU	8×8
3	CONV-(3, 3, n), stride (1, 1) — ReLU	8×8
4	CONV-(3, 3, n), stride (1, 1) — ReLU	8×8
5	CONV-(3, 3, n), stride (1, 1) — ReLU — POOL-(3, 3), stride (2, 2)	4×4
6	CONV-(3, 3, n), stride (1, 1) — ReLU	4×4
7	CONV-(3, 3, n), stride (1, 1) — ReLU — POOL-(3, 3), stride (2, 2)	2×2
8	FC-(10, $4n$)	—

Table 1: Structure of the CNNs. Here CONV-(s, s, n) is a convolutional layer with a receptive field size of s and n filters. POOL-(s, s) is the max pooling operation over a spatial region of size $s \times s$. Stride (s, s) is the stride of size s in each dimension, applied to the accompanied operation. FC-(10, $4n$) is a fully-connected layer with dimensions $10 \times 4n$. ReLU indicates an entry-wise rectifier linear unit nonlinearity. All layers have trainable biases. We apply appropriate paddings to obtain the corresponding output spatial dimension.

the \otimes operator. Recall that this summation structure is key to the self-averaging property in light of Eq. (25). The only difference is that local operations (such as the $*$ operator) are no longer scalar-valued, but rather vector-valued (or matrix-valued). As discussed in Section 2.4, we expect that this difference is not very critical and the MF limit behavior still occurs, provided that the number of filters $n_\ell \rightarrow \infty$ while all other dimensions are kept constant. The scalings can be deduced from Section 3.1.

In the following, we present an experimental validation of the existence of the MF limit in multilayer CNNs on the CIFAR-10 classification task. We construct 8-layers networks according to Table 1. Note that we apply a stride of size (2, 2) in the first two layers, which reduces the spatial dimensions by a considerable amount and hence limits memory consumption at the cost of the networks’ performance. We use the same number of filters at each layer n , where n is to be varied among the networks. We normalize each RGB value in the image to the range $[-1, +1]$. We use the cross-entropy loss \mathcal{L} , and use the whole training set of size 50×10^3 . To train the networks, we use mini-batch SGD with an annealed learning rate $\alpha_k = 0.08k^{-0.1}$, where $k \geq 1$ is the SGD iteration, and a batch size of 100. We initialize the networks in a similar fashion to those in Section 4.2, i.e. the first layer weight entries are initialized with $\mathbf{N}(0, 2/(9d))$, the other layers’ weight entries are initialized with $\mathbf{N}(1, 0.1)$, and all biases are initialized to zero.

The result is shown in Fig. 12. We observe the good match among the networks – the larger n , the better match. The performance is also realistic: the test error rate for the network with $n = 400$ is about 27%. This is similar to the performance of a 259-layers CNN reported in [XBSD⁺18], which attains a test error rate of 30%. It has a similar vanilla structure, is initialized with i.i.d. Gaussian weights of zero mean and carefully selected variance, is trained without regularization, but is not under our scalings. Hence the introduced scalings do not trivialize the performance of the networks.

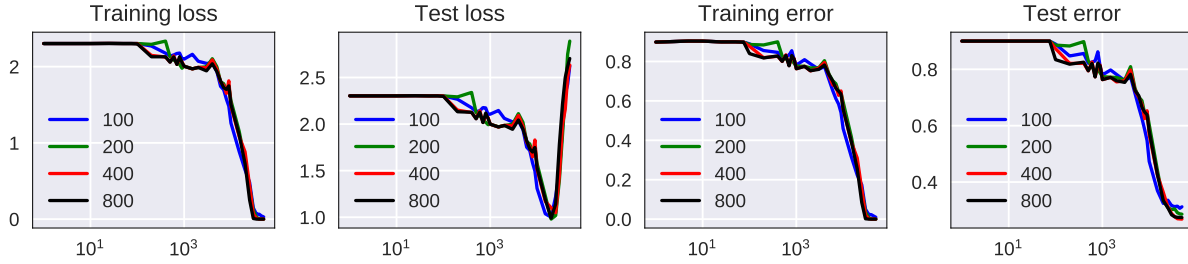


Figure 12: The performance of 8-layers CNNs on CIFAR-10 classification, plotted against training iteration. For each network, $n = 100, 200, 400, 800$ respectively.

References

- [ABGM14] Sanjeev Arora, Aditya Bhaskara, Rong Ge, and Tengyu Ma, *Provable bounds for learning some deep representations*, International Conference on Machine Learning, 2014, pp. 584–592.
- [AZLL18] Zeyuan Allen-Zhu, Yuanzhi Li, and Yingyu Liang, *Learning and generalization in overparameterized neural networks, going beyond two layers*, arXiv preprint arXiv:1811.04918 (2018).
- [AZLS18] Zeyuan Allen-Zhu, Yuanzhi Li, and Zhao Song, *A convergence theory for deep learning via over-parameterization*, arXiv preprint arXiv:1811.03962 (2018).
- [BRV⁺06] Yoshua Bengio, Nicolas L Roux, Pascal Vincent, Olivier Delalleau, and Patrice Marquette, *Convex neural networks*, Advances in neural information processing systems, 2006, pp. 123–130.
- [CB18a] Lenaïc Chizat and Francis Bach, *A note on lazy training in supervised differentiable programming*, arXiv preprint arXiv:1812.07956 (2018).
- [CB18b] L  na  c Chizat and Francis Bach, *On the global convergence of gradient descent for over-parameterized models using optimal transport*, Advances in Neural Information Processing Systems, 2018, pp. 3040–3050.
- [CHM⁺15] Anna Choromanska, Mikael Henaff, Michael Mathieu, G  rard Ben Arous, and Yann LeCun, *The loss surfaces of multilayer networks*, Artificial Intelligence and Statistics, 2015, pp. 192–204.
- [Coo18] Yaim Cooper, *The loss landscape of overparameterized neural networks*, arXiv preprint arXiv:1804.10200 (2018).
- [CPS18] Minmin Chen, Jeffrey Pennington, and Samuel Schoenholz, *Dynamical isometry and a mean field theory of RNNs: Gating enables signal propagation in recurrent neural networks*, Proceedings of the 35th International Conference on Machine Learning, vol. 80, 2018, pp. 873–882.

- [dGMHR⁺18] Alexander G. de G. Matthews, Jiri Hron, Mark Rowland, Richard E. Turner, and Zoubin Ghahramani, *Gaussian process behaviour in wide deep neural networks*, International Conference on Learning Representations, 2018.
- [DL18] Simon Du and Jason Lee, *On the power of over-parametrization in neural networks with quadratic activation*, Proceedings of the 35th International Conference on Machine Learning, vol. 80, 2018, pp. 1329–1338.
- [DLL⁺18] Simon S Du, Jason D Lee, Haochuan Li, Liwei Wang, and Xiyu Zhai, *Gradient descent finds global minima of deep neural networks*, arXiv preprint arXiv:1811.03804 (2018).
- [DZPS19] Simon S. Du, Xiyu Zhai, Barnabas Poczos, and Aarti Singh, *Gradient descent provably optimizes over-parameterized neural networks*, International Conference on Learning Representations, 2019.
- [FB17] C Daniel Freeman and Joan Bruna, *Topology and geometry of half-rectified network optimization*, International Conference on Learning Representations (2017).
- [GARA19] Adrià Garriga-Alonso, Carl Edward Rasmussen, and Laurence Aitchison, *Deep convolutional networks as shallow gaussian processes*, International Conference on Learning Representations, 2019.
- [GJS⁺19] Mario Geiger, Arthur Jacot, Stefano Spigler, Franck Gabriel, Levent Sagun, Stéphane d’Ascoli, Giulio Biroli, Clément Hongler, and Matthieu Wyart, *Scaling description of generalization with number of parameters in deep learning*, arXiv preprint arXiv:1901.01608 (2019).
- [GSd⁺18] Mario Geiger, Stefano Spigler, Stéphane d’Ascoli, Levent Sagun, Marco Baity-Jesi, Giulio Biroli, and Matthieu Wyart, *The jamming transition as a paradigm to understand the loss landscape of deep neural networks*, arXiv preprint arXiv:1809.09349 (2018).
- [Han18] Boris Hanin, *Which neural net architectures give rise to exploding and vanishing gradients?*, Advances in Neural Information Processing Systems 31, 2018, pp. 580–589.
- [HJ15] Tamir Hazan and Tommi Jaakkola, *Steps toward deep kernel methods from infinite neural networks*, arXiv preprint arXiv:1508.05133 (2015).
- [HNP⁺18] Nhat Ho, Tan Nguyen, Ankit Patel, Anima Anandkumar, Michael I Jordan, and Richard G Baraniuk, *Neural rendering model: Joint generation and prediction for semi-supervised learning*, arXiv preprint arXiv:1811.02657 (2018).
- [HR18] Boris Hanin and David Rolnick, *How to start training: The effect of initialization and architecture*, Advances in Neural Information Processing Systems 31, 2018, pp. 569–579.
- [JGH18] Arthur Jacot, Franck Gabriel, and Clement Hongler, *Neural tangent kernel: Convergence and generalization in neural networks*, Advances in Neural Information Processing Systems 31, 2018, pp. 8580–8589.

- [JMM19] Adel Javanmard, Marco Mondelli, and Andrea Montanari, *Analysis of a two-layer neural network via displacement convexity*, arXiv preprint arXiv:1901.01375 (2019).
- [LBH15] Yann LeCun, Yoshua Bengio, and Geoffrey Hinton, *Deep learning*, nature **521** (2015), no. 7553, 436.
- [LL18] Yuanzhi Li and Yingyu Liang, *Learning overparameterized neural networks via stochastic gradient descent on structured data*, Advances in Neural Information Processing Systems, 2018, pp. 8168–8177.
- [LN19] Ping Li and Phan-Minh Nguyen, *On random deep weight-tied autoencoders: Exact asymptotic analysis, phase transitions, and implications to training*, International Conference on Learning Representations, 2019.
- [LSdP⁺18] Jaehoon Lee, Jascha Sohl-dickstein, Jeffrey Pennington, Roman Novak, Sam Schoenholz, and Yasaman Bahri, *Deep neural networks as gaussian processes*, International Conference on Learning Representations, 2018.
- [Mal16] Stéphane Mallat, *Understanding deep convolutional networks*, Philosophical Transactions of the Royal Society A: Mathematical, Physical and Engineering Sciences **374** (2016), no. 2065, 20150203.
- [MBM18] Song Mei, Yu Bai, and Andrea Montanari, *The landscape of empirical risk for non-convex losses*, The Annals of Statistics **46** (2018), no. 6A, 2747–2774.
- [MMN18] Song Mei, Andrea Montanari, and Phan-Minh Nguyen, *A mean field view of the landscape of two-layers neural networks*, Proceedings of the National Academy of Sciences, vol. 115, 2018, pp. 7665–7671.
- [MP16] Hrushikesh N Mhaskar and Tomaso Poggio, *Deep vs. shallow networks: An approximation theory perspective*, Analysis and Applications **14** (2016), no. 06, 829–848.
- [NH17] Quynh Nguyen and Matthias Hein, *The loss surface of deep and wide neural networks*, Proceedings of the 34th International Conference on Machine Learning, vol. 70, 2017, pp. 2603–2612.
- [NH18] Quynh Nguyen and Matthias Hein, *Optimization landscape and expressivity of deep cnns*, International Conference on Machine Learning, 2018, pp. 3727–3736.
- [NXB⁺19] Roman Novak, Lechao Xiao, Yasaman Bahri, Jaehoon Lee, Greg Yang, Daniel A. Abolafia, Jeffrey Pennington, and Jascha Sohl-dickstein, *Bayesian deep convolutional networks with many channels are gaussian processes*, International Conference on Learning Representations, 2019.
- [PLR⁺16] Ben Poole, Subhaneil Lahiri, Maithra Raghu, Jascha Sohl-Dickstein, and Surya Ganguli, *Exponential expressivity in deep neural networks through transient chaos*, Advances in neural information processing systems, 2016, pp. 3360–3368.
- [PSG17] Jeffrey Pennington, Samuel Schoenholz, and Surya Ganguli, *Resurrecting the sigmoid in deep learning through dynamical isometry: theory and practice*, Advances in neural information processing systems, 2017, pp. 4785–4795.

- [RDS⁺15] Olga Russakovsky, Jia Deng, Hao Su, Jonathan Krause, Sanjeev Satheesh, Sean Ma, Zhiheng Huang, Andrej Karpathy, Aditya Khosla, Michael Bernstein, Alexander Berg, and Fei-Fei Li, *Imagenet large scale visual recognition challenge*, International Journal of Computer Vision **115** (2015), no. 3, 211–252.
- [RVE18] Grant M Rotskoff and Eric Vanden-Eijnden, *Neural networks as interacting particle systems: Asymptotic convexity of the loss landscape and universal scaling of the approximation error*, arXiv preprint arXiv:1805.00915 (2018).
- [SC16] Daniel Soudry and Yair Carmon, *No bad local minima: Data independent training error guarantees for multilayer neural networks*, arXiv preprint arXiv:1605.08361 (2016).
- [SGd⁺18] Stefano Spigler, Mario Geiger, Stéphane d’Ascoli, Levent Sagun, Giulio Biroli, and Matthieu Wyart, *A jamming transition from under- to over-parametrization affects loss landscape and generalization*, arXiv preprint arXiv:1810.09665 (2018).
- [SGGSD17] Samuel S Schoenholz, Justin Gilmer, Surya Ganguli, and Jascha Sohl-Dickstein, *Deep information propagation*, International Conference on Learning Representations (2017).
- [SJL18] Mahdi Soltanolkotabi, Adel Javanmard, and Jason D Lee, *Theoretical insights into the optimization landscape of over-parameterized shallow neural networks*, IEEE Transactions on Information Theory (2018).
- [SS16] Itay Safran and Ohad Shamir, *On the quality of the initial basin in overspecified neural networks*, International Conference on Machine Learning, 2016, pp. 774–782.
- [SS18a] Justin Sirignano and Konstantinos Spiliopoulos, *Mean field analysis of neural networks*, arXiv preprint arXiv:1805.01053 (2018).
- [SS18b] ———, *Mean field analysis of neural networks: A central limit theorem*, arXiv preprint arXiv:1808.09372 (2018).
- [SZ15] Karen Simonyan and Andrew Zisserman, *Very deep convolutional networks for large-scale image recognition*, International Conference on Learning Representations (2015).
- [SZT17] Ravid Shwartz-Ziv and Naftali Tishby, *Opening the black box of deep neural networks via information*, arXiv preprint arXiv:1703.00810 (2017).
- [VBB18] Luca Venturi, Afonso Bandeira, and Joan Bruna, *Spurious valleys in two-layer neural network optimization landscapes*, arXiv preprint arXiv:1802.06384 (2018).
- [WLLM18] Colin Wei, Jason D Lee, Qiang Liu, and Tengyu Ma, *On the margin theory of feedforward neural networks*, arXiv preprint arXiv:1810.05369 (2018).
- [XBSD⁺18] Lechao Xiao, Yasaman Bahri, Jascha Sohl-Dickstein, Samuel Schoenholz, and Jeffrey Pennington, *Dynamical isometry and a mean field theory of CNNs: How to train 10,000-layer vanilla convolutional neural networks*, Proceedings of the 35th International Conference on Machine Learning, vol. 80, 2018, pp. 5393–5402.

- [YPR⁺19] Greg Yang, Jeffrey Pennington, Vinay Rao, Jascha Sohl-Dickstein, and Samuel S. Schoenholz, *A mean field theory of batch normalization*, International Conference on Learning Representations, 2019.
- [YS17] Ge Yang and Samuel Schoenholz, *Mean field residual networks: On the edge of chaos*, Advances in neural information processing systems, 2017, pp. 7103–7114.
- [YSJ19] Chulhee Yun, Suvrit Sra, and Ali Jadbabaie, *Small nonlinearities in activation functions create bad local minima in neural networks*, International Conference on Learning Representations, 2019.
- [ZCZG18] Difan Zou, Yuan Cao, Dongruo Zhou, and Quanquan Gu, *Stochastic gradient descent optimizes over-parameterized deep relu networks*, arXiv preprint arXiv:1811.08888 (2018).
- [ZSJ⁺17] Kai Zhong, Zhao Song, Prateek Jain, Peter L. Bartlett, and Inderjit S. Dhillon, *Recovery guarantees for one-hidden-layer neural networks*, Proceedings of the 34th International Conference on Machine Learning, vol. 70, 2017, pp. 4140–4149.